Universidade Nova de Lisboa
Faculdade de Ciências e Tecnologia

Master Dissertation

Integrated Master on Biomedical Engineering

Detection of Purkinje Images for Automatic Positioning of Fixation Target and Interferometric Measurements of Anterior Eye Chamber

Mariana Quelhas Dias Rodrigues Almeida
(student number 23279)

Winter Semester 2011/12
20th of April, 2012

Universidade Nova de Lisboa
Faculdade de Ciências e Tecnologia

Master Dissertation

Detection of Purkinje Images for Automatic Positioning of Fixation Target and Interferometric Measurements of Anterior Eye Chamber

Mariana Quelhas Dias Rodrigues Almeida (student number 23279)

Adviser: Prof. Rainer Leitgeb, Medical University of Vienna
Co-Adviser: Prof. Branislav Grajciar, Medical University of Vienna

Work presented as part of the Integrated Master on Biomedical Engineering, as parcial requirement for a Master degree in Biomedical Engineering.

Winter Semester 2011/12
20th of April, 2012

Acknowledgements

To Professor Rainer Leitgeb, whose guidance and knowledge were an inspiration.
To Professor Branislav Grajciar, on whose guidance I relied and from whom I learned so much.
To my parents, for their support and help along this path.
To João, for his support and inspiration.

Abstract

In cataract surgery, the eye's natural lens is removed because it has gone opaque and doesn't allow clear vision any longer. To maintain the eye's optical power, a new artificial lens must be inserted. Called Intraocular Lens (IOL), it needs to be modelled in order to have the correct refractive power to substitute the natural lens.

Calculating the refractive power of this substitution lens requires precise anterior eye chamber measurements. An interferometry equipment, the AC Master from Zeiss Meditec, AG, was in use for half a year to perform these measurements. A Low Coherence Interferometry (LCI) measurement beam is aligned with the eye's optical axis, for precise measurements of anterior eye chamber distances. The eye follows a fixation target in order to make the visual axis align with the optical axis. Performance problems occurred, however, at this step. Therefore, there was a necessity to develop a new procedure that ensures better alignment between the eye's visual and optical axes, allowing a more user friendly and versatile procedure, and eventually automatizing the whole process.

With this instrument, the alignment between the eye's optical and visual axes is detected when Purkinje reflections I and III are overlapped, as the eye follows a fixation target.

In this project, image analysis is used to detect these Purkinje reflections' positions, eventually automatically detecting when they overlap.

Automatic detection of the third Purkinje reflection of an eye following a fixation target is possible with some restrictions. Each pair of detected third Purkinje reflections is used in automatically calculating an acceptable starting position for the fixation target, required for precise measurements of anterior eye chamber distances.

Keywords: Fixation target, Image analysis, Eye's optical and visual axis, Low Coherence Interferometry (LCI), Purkinje reflections, (Eye length) IOL measurements

Resumo

Na cirurgia da catarata, a lente natural do olho é retirada por se ter tornado opaca e já não permitir uma visão clara. Para manter o poder óptico do olho é necessário inserir uma nova lente artificial. Esta lente, designada por Intraocular Lens - IOL (lente intraocular), em inglês, precisa de ser modelada de forma a ter o poder refractivo correcto para tomar o lugar da lente natural.

O cálculo do poder refractivo da lente de substituição requere medições precisas da câmara anterior do olho. Um instrumento de medição interferométrica, o AC Master da Zeiss Meditec, AG, esteve em uso durante meio ano para realizar estas medições. Um feixe de medição de Low Coherence Interferometry - LCI (interferometria de baixa coerência), em inglês, é alinhado com eixo óptico do olho, para realização de medições precisas de distâncias da câmara anterior do olho.

O olho segue um alvo de fixação, garantindo alinhamento entre o eixo visual e o eixo óptico do olho. O instrumento padecia de problemas de performance neste alinhamento. Surge então a necessidade de desenvolver um novo procedimento que garanta melhor alinhamento entre os eixos visual e óptico do olho, permitindo um procedimento mais acessível e versátil, e eventualmente automatizar todo o processo.

Com este instrumento, o alinhamento entre os eixos visual e óptico do olho é detectado quando os reflexos I e III de Purkinje se sobrepõem, à medida que o olho segue um alvo de fixação.

Neste projecto, utiliza-se análise de imagem para detectar a posição destes reflexos de Purkinje e eventualmente verificar automaticamente quando estes se sobrepõem.

A detecção automática do terceiro reflexo de Purkinje de um olho que segue um alvo de fixação é possível com algumas restrições. Cada par de terceiro reflexos de Purkinje detectados é usado no cálculo automático de um ponto de partida aceitável para a localização do alvo de fixação, necessário para medições precisas da câmara anterior do olho.

Palavras-chave: Alvo de fixação, Análise de imagem, Eixos óptico e visual do olho, Interferometria de Baixa Coerência (LCI), Reflexos de Purkinje, Medições para IOL (distâncias intra-oculares)

Contents

1 Introduction **1**
- 1.1 Project Context 1
- 1.2 Document Overview 2

2 Theoretical Framework **3**
- 2.1 Purkinje Images 3
- 2.2 Eye's Optical and Visual Axes 5
- 2.3 The AC Master 6
  - 2.3.1 Short Instrument Description 6
  - 2.3.2 Basic Operation 7
- 2.4 Interferometry Measurements 9
- 2.5 Project Overview 12
- 2.6 State of the Art 13
  - 2.6.1 Wave Interference Technology 13
  - 2.6.2 Scheimpflug-based Imaging 14

3 Materials and Methods **17**
- 3.1 Introduction 17
- 3.2 Aligning Subject and Instrument for Image Capturing 18
- 3.3 Capturing Images for Analysis 21
  - 3.3.1 Following the Fixation Target Pattern 21
  - 3.3.2 Image Capturing 22
- 3.4 Image Analysis 23
  - 3.4.1 Image Features 23
    - 3.4.1.1 Static 23
    - 3.4.1.2 Motion-related Features 25
  - 3.4.2 Final Procedure 26
- 3.5 Automatic Target Positioning 27
  - 3.5.1 OLED Rotation 29
    - 3.5.1.1 Measurements 29
    - 3.5.1.2 Data Analysis 30
  - 3.5.2 Purkinje Reflections Separation vs. Eye Tilt 31
    - 3.5.2.1 Measurements 31
    - 3.5.2.2 Data Analysis 33
  - 3.5.3 Eye Fixation Deviation 34
  - 3.5.4 Final Calculations 35

4 Related Work **39**
4.1 Searching for an Optimal Image Analysis Procedure 39
4.1.1 Pre-Analysis 39
4.1.2 Detecting the Third Purkinje Reflection 41
4.1.2.1 Object Detection in Matlab 41
4.1.2.2 Foreground/Background Differentiation 41
4.1.2.3 Shape Differentiation 43
4.2 Results and Discussion 45

5 Results **47**
5.1 Image Analysis 47
5.1.1 Final Procedure 47
5.1.2 Detection Problems 51
5.2 Automatic Target Positioning 52
5.2.1 OLED Rotation 52
5.2.2 Purkinje Reflections Separation vs. Eye Tilt 53
5.2.2.1 Angle Step Calculation 53
5.2.2.2 Analysing the Results 54
5.2.3 Eye Fixation Deviations 57
5.2.4 Final Calculations 58

6 Discussion **59**
6.1 Image Analysis 59
6.2 Automatic Target Positioning 61
6.2.1 Purkinje Reflections Separation vs. Eye Tilt 61
6.2.2 Final Calculations 63

7 Conclusions and Future Work **65**

List of Figures

1.1 Schematic representation of the eye. After [8]. 1

2.1 Formation of Purkinje reflections. 4
2.2 Optical axes of the eye and important angles: [AR] - optical axis; [OF] - visual axis; [OC] - fixation axis; angle α, O$\hat{\text{N}}$A, between optical and visual axes; angle κ, O$\hat{\text{P}}$A, between optical axis and pupillary line [OP]; angle γ, O$\hat{\text{C}}$A, between optical and fixation axes. From [14]. 5
2.3 Operator's view of the AC Master. From [22]. 7
2.4 AC Master's keyboard. From [22]. 7
2.5 Patient's view of the AC Master. From [22]. 8
2.6 Electric field distribution around the focus of a Gaussian laser beam. Upper image: perfect spatial and time coherence; Lower image: high spatial coherence, poor time coherence. 9
2.7 Basic set-up of a dual beam partial coherence interferometer. From [15]. 10
2.8 Measurement example. From [22]. 11
2.9 Ultrasound biometry procedure set-up. From [2]. 13
2.10 Scheimpflug principle. From [17]. 14
2.11 Scheimpflug-based imaging. 15

3.1 WtW measurement mode screen: 1 - Display field for results of right eye; 2 - Live video image; 3 - Display field for results of left eye; 4 - Status, first name, name, measuring mode and eye (right/left) of live image. From [22]. 19
3.2 WtW alignment: 1 - Image of fixation point; 2 - Image of illumination LED (reflection point). From [22]. 19
3.3 ACD measurement mode, for Purkinje reflections alignment: 1 - Reflection from anterior corneal surface; 2 - Reflection from posterior lens surface; 3 - Reflection from anterior lens surface; 4 - Position of fixation target on internal LC display. From [22]. 20
3.4 Programmed target shape. 21
3.5 Example of captured image. 22
3.6 Most common artefacts. 24
3.7 Sporadic artefacts. 24
3.8 Artefacts resulting from misalignment. 24
3.9 Misalignment examples. 25
3.10 3P appearing within consecutive frames. 25
3.11 Procedure to make detected third Purkinje reflection (green outline) follow arrow's path, so that it overlaps first Purkinje reflection 27
3.12 Dependencies between movements in predicting third Purkinje reflection movement. 28

3.13 Programmed line in Labview to test OLED rotation. 29
3.14 Programmed line's starting and final positions for OLED rotation calculation. 30
3.15 Test eye and goniometer mounted in the AC Master for eye tilt measurements. 31
3.16 Measuring test eye tilt. 33
3.17 Third Purkinje location changes with fixed target. 34
3.18 Transforming $\vec{d_{pt}}$ into $\vec{d_{Op}}$, and $\vec{d_{Op}}$ into $\vec{d_{3P}}$. 37
3.19 $\vec{d_{pt}}$ gives $\vec{d_{3P}}$ through rotation by ϕ and scaling by β. 37

4.1 Variance filter on original image. 40
4.2 Grayscale values along depicted yellow line, before and after static level thresholding. 40
4.3 Connected components object detection. 41
4.4 Detected objects for inter-frame connectivity. 42
4.5 Original frames example considered for NCC. Grid pattern for NCC also shown. First Purkinje reflection can be seen to move slightly. 43
4.6 Detected third Purkinje reflections. 43
4.7 Eccentricity values to distinguish between first Purkinje reflections. 44
4.8 Detected regions with movement. 45

5.1 Reading image into Matlab. 47
5.2 Coarse first and third Purkinje reflections separation. 48
5.3 Isolating first Purkinje reflection. 48
5.4 Cropping area of interest. 49
5.5 Isolating third Purkinje reflection. 49
5.6 Third Purkinje reflection detection final criteria. 50
5.7 Detection in misalignment. 51
5.8 Other detection problems. 51
5.9 Separation between first and third Purkinje reflections as a resul of test eye tilting. 55
5.10 Distance vs. Absolute angle. 55
5.11 Detected third Purkinje reflection's location with fixed target. 57
5.12 Calculated vs. Original target locations, detail. 58

6.1 Comparing separation vs. absolute angle tilt with θ and sin (θ) plots. 62

List of Tables

2.1 Measurement modes and their symbols. From [22]. 6

4.1 Methods and main results for background/foreground differentiation approach. 42

5.1 Measurements and results for OLED rotation angle calculations. 52
5.2 Measurements and results for angle step calculations. 53
5.3 Linear regression coefficients for horizontal and vertical movements' plots. 56
5.4 Statistics for third Purkinje location as the eye looks at a fixed target. 57

6.1 Third Purkinje detection and adequate target location calculation efficiency rates. 59

1. Introduction

1.1 Project Context

Replacement of the opaque crystalline lens in cataract surgery with an Intra Ocular Lens (IOL) requires intra ocular measurements to calculate the refractive power of the replacement IOL. These measurements include axial eye length, anterior chamber depth along the optical axis as well as measurement of the refractive power of the cornea. Precise interferometry measurements of the anterior eye chamber are important for refractive power calculations. Dual beam Low Coherence Interferometry (LCI) is used for these measurements, where alignment of the measurement beam with the eye's optical axis is of most importance, in order to achieve good measurement sensitivity.

Detection of this axis' orientation is made with help of Purkinje reflections [1]. When they overlap, there is alignment of the eye's optical axis and the illumination beam, and only then can the interferometry measurement beam be used to perform measurements along this same axis with higher sensitivity.

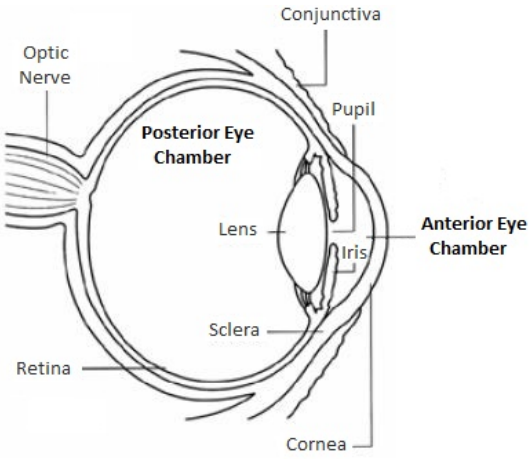

Figure 1.1: Schematic representation of the eye. After [8].

The AC Master from Zeiss Meditec, AG is the instrument used for anterior eye chamber calculations of cataract surgery patients. It incorporates interferometry instrumentation for anterior eye chamber depth measurements, illumination beam apparatus in order to create Purkinje reflections and a computer connection.

It was used for some time in clinical practice, however there were performance problems concerning alignment between the eye's optical and visual axes. This alignment is detected when the first and third Purkinje reflections overlap (further explained in next chapter). An

[1] In this document, to avoid misinterpretations between a digital image and corneal and lens' reflections, the latter are called Purkinje *reflections* instead of the most common denomination Purkinje *images*.

operator watches the reflections' position in the instruments' external display and makes an interferometry measurement whenever they align. This process has problems in two ways:

- **There is a need for a skilled operator (physician).** Only an operator who can correctly identify the different Purkinje reflections and tell them apart from other artefacts in the image can perform this task. This results in high specialization of this work and limits the availability of this procedure, even for cooperative patients.
- **Detecting the alignment might not always result in a precise measurement.** Involuntary eye movements as well as natural lens tilt lead to a great deal of instability on the Purkinje reflections' location. Therefore, when the operator is making the interferometry measurement, the reflections might have moved again, which leads to axes' misalignment during measurement and incorrect results.

In conclusion, the process was very unstable resulting in an inability to consistently achieve correct alignment. Therefore, the resulting measurements were unreliable. A new procedure that could more efficiently detect the Purkinje images' alignment was required.

This project was created in order to research whether such a procedure is possible.

1.2 Document Overview

An introductory chapter will give a succinct review of the instrument's internal optics, as well as an explanation on Purkinje reflections, along with a brief introduction on the required interferometry measurements. A short current state of the art topic is also given. The next chapter will explain all steps that were taken in this project to help improve the AC Master from Zeiss Meditec, AG, including image capturing, image analysis, as well as other ideas that proved useful for this project's development. In the following two chapters, the results from those procedures will be presented and discussed. Finally, a concluding chapter will aim at showing how the AC Master from Zeiss Meditec, AG can continue to be used and which steps can be taken for that to happen.

2. Theoretical Framework

In order to understand this project's approach, first a brief introduction to Purkinje reflections will be given in this chapter, along with a short explanation on the necessary measurements, followed by a succinct overview of the AC Master's components and its performance.

Finally, after having presented this theoretical basis, this project's approach to the given problem will be laid out.

2.1 Purkinje Images

Purkinje images are formed when light hits the eye's optical structures. They take their name after Czech anatomist and physiologist Ján Purkyně who first described them.

When light hits the eye, the eye's optical structures reflect the light back. Since there are four optical structures in the eye, which form the cornea and lens, there are also four light reflections, known as Purkinje images number 1, 2, 3 and 4. Figure 2.1(b) shows how they are formed.

- The first two come from the convex surfaces of the anterior and posterior corneal surfaces.
- The third and fourth come from the posterior convex lens' surface and anterior concave lens' surface, respectively.
- The first three are erect and virtual images, whereas the fourth image is real and inverted [14].

Looking at an eye in normal day light allows the observer to see the first Purkinje image (coming from the anterior surface of the cornea) on the cornea itself. The other images are normally not visible. To see the other images there mustn't be much light surrounding the eye, therefore a single illumination beam is the best choice to see the most Purkinje reflections. Figure 2.1(a) shows such an example, a typical Purkinje images image taken with the AC Master.

The first Purkinje image is clearly visible, as well as the third one. The second reflection is overlapping the first one and cannot be distinguished. The fourth reflection is not visible; either it is too dim to be seen or the illumination beam's angle doesn't make it possible to be seen. This occurs with most experiments that were performed, therefore the fourth Purkinje reflection will not be discussed in this work. In this work, the first and third Purkinje reflections are the most important.

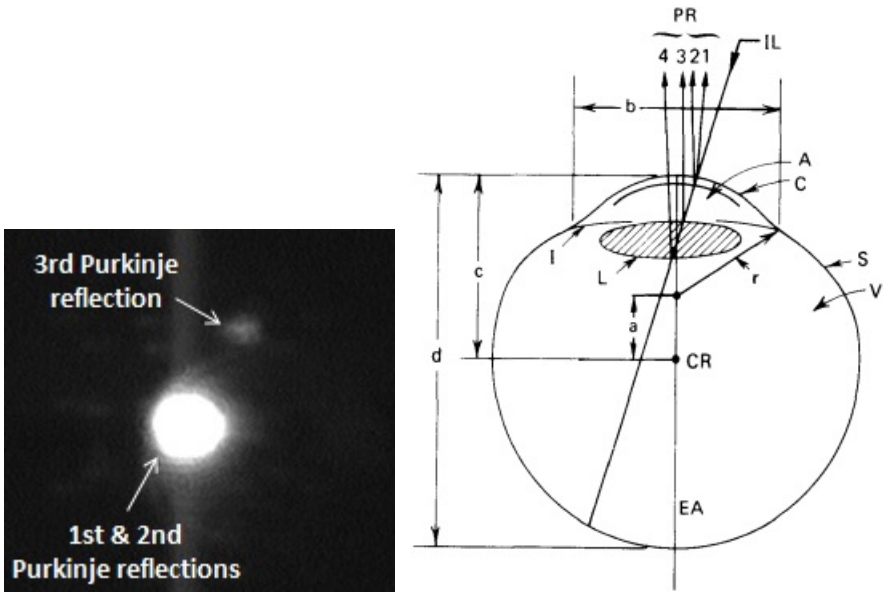

(a) Purkinje images created with a single illumination beam.

(b) Schematic diagram of the eye. IL - incoming light; A - aqueous; C - cornea; S - sclera; V - vitreous; I - iris; L - lens; CR - center of rotation; EA - eye axis (optical axis). Visual axis not depicted. From [7].

Figure 2.1: Formation of Purkinje reflections.

2.2 Eye's Optical and Visual Axes

An optical axis is defined as the line that connects the centres of reflection and refraction of a centred system. Since the eye is not a centred system, the optical axis is defined as the "best fit" line through the centres of curvature of each reflecting and refracting surface within the eye. For the eye, its optical axis is defined as the line connecting the cornea and lens's centres of curvature (Figure 2.2). Therefore, the Purkinje reflections' relative positions are a consequence of the optical axis' direction relative to the illumination beam [7].

Making the measurement beam go along the same direction as the illumination beam ensures that when optical axis and illumination beam align, measurement beam and optical axis alignment also occurs. Since the measurement beam is just outside human visible range (850 nm), only the illumination beam is visible to the patient (and only its reflections are seen by the operator).

On the other hand, alignment between the illumination and eye's optical axes needs to be detected, which is done by an external operator, in order to know when to perform a measurement. This alignment setup is achieved by making the patient look at a target. Making the target a single pixel, it also serves the purpose of illumination beam.

The operator can now see the Purkinje reflections, however, only when visual axis and optical axis are close to alignment, meaning that the angle between (known as α - Figure 2.2) them must be very small (results from section 5.2.2 indicate $\sim 1{,}7°$). In this project, ideally, the patient needs to look in a direction where first and third Purkinje reflections overlapping occurs. This means that the patient's visual and optical axes are aligned (α is zero).

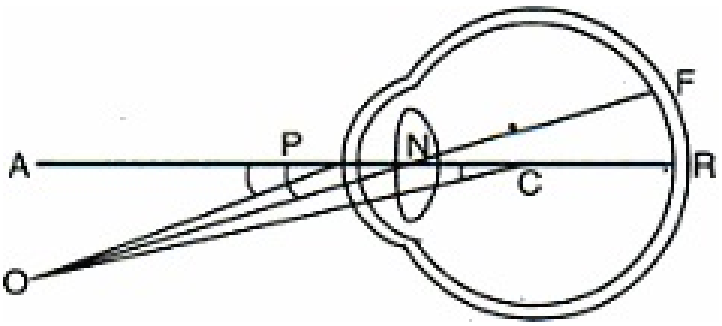

Figure 2.2: Optical axes of the eye and important angles: [AR] - optical axis; [OF] - visual axis; [OC] - fixation axis; angle α, O$\hat{\text{N}}$A, between optical and visual axes; angle κ, O$\hat{\text{P}}$A, between optical axis and pupillary line [OP]; angle γ, O$\hat{\text{C}}$A, between optical and fixation axes. From [14].

2.3 The AC Master

2.3.1 Short Instrument Description

The AC Master is a biometry instrument that measures parameters of the anterior segment of the human eye. They include corneal thickness, Anterior Chamber Depth (ACD), lens thickness and eye white width (known as white to white (WtW) measurement). This project concerns the procedure for ACD measurements. The ACD is taken as the distance between posterior corneal surface and anterior lens surface (see Figure 1.1).

These measurements are performed based on optical interference, using a method known as Partial Coherence Interferometry (PCI). It allows detection of interfaces inside the eye, much like an ultrasound A-scan. They are, however, non-contact and much more precise than previous ultrasound methods used for the same purpose[10], [15] (see section 2.4).

In order to perform ACD distance measurements, optical and measurement beam alignment, as well as eye's optical and visual axes alignment must occur (section 2.2). For the latter, the instrument contains an OLED display which serves for target display, that controls the patient's fixation direction.

Inside the AC Master there is a CCD camera for observation of the patient's eye. A backlit external LC display (Figure 2.3, 2) allows observation of the patient's eye and display of results.

There are two possible eye illumination modes, accounting for three measurement modes. Table 2.1 summarizes them.

Table 2.1 Measurement modes and their symbols. From [22].

Measurement Mode	Symbol	Observable	Illumination	Example
Pachymeter		Anterior surface of the eye	LEDs around exit aperture	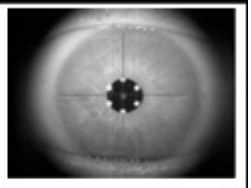
WtW				
ACD		Purkinje reflections	LED inside instrument	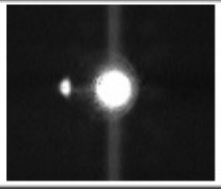

The AC Master's control computer runs on Windows XP, and is keyboard controlled (2.4). It can also be connected to another computer, for program and interface development (Figure 2.3, 1).

2.3.2 Basic Operation

The patient rests his head and chin on the instrument's headrest (Figure 2.5, 4 and 6). The operator uses WtW or pachymeter mode in order to roughly align instrument and eye. More precise alignment of measurement beam and eye's optical axis is performed in ACD mode, where Purkinje images are observed.

Alignment is initially done with a vertical headrest control (Figure 2.5, 2), in order to very coarsely align the eye with the measurement beam's exit aperture (Figure 2.5, 7). Afterwards, fine alignment is done through aid of a joystick that moves the instrument in X,Y and Z directions (Figure 2.3, 1).

An external measurement trigger button performs interferometry measurements when pressed (not depicted in Figures 2.3-2.5). Therefore, when the operator decides that adequate alignment is achieved, the button is pressed and a measurement is produced (details on measurements in section 2.4).

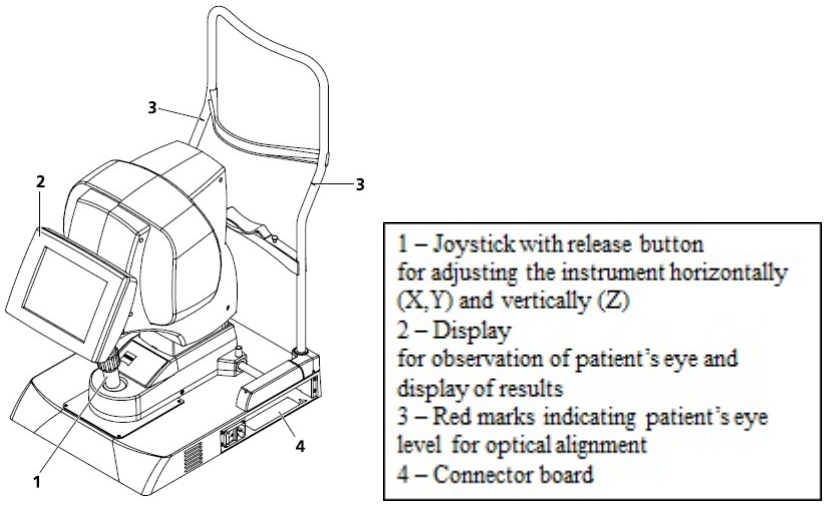

Figure 2.3: Operator's view of the AC Master. From [22].

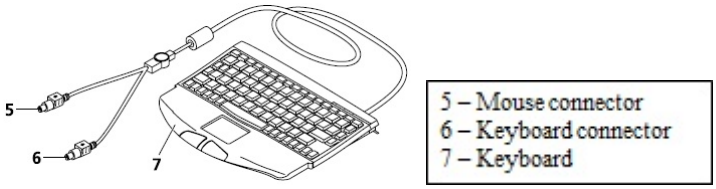

Figure 2.4: AC Master's keyboard. From [22].

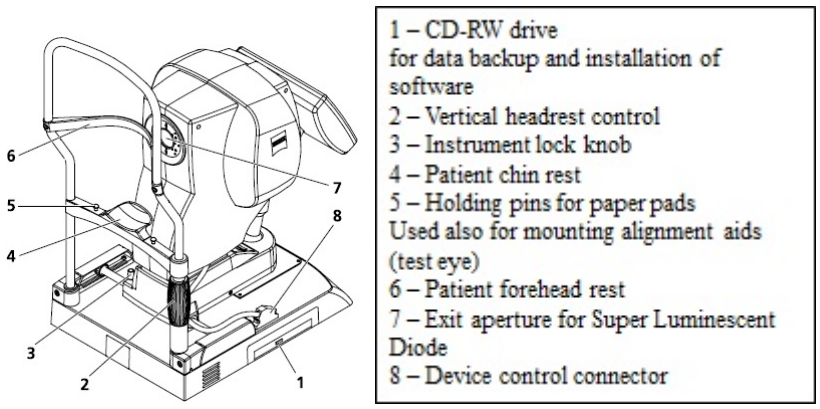

Figure 2.5: Patient's view of the AC Master. From [22].

2.4 Interferometry Measurements

The AC Master performs dual beam interferometry measurements in the eye. This is a type of PCI, using low coherence light from a Super Luminescent Diode (SLD), with 850nm/450 μW, to detect interfaces that separate media of different refractive indices within the studied object.

Interferometry is a measurement process that relies on splitting a broadband light source and recombining it again to detect interference patterns after recombination. Spatial and time coherence of the scanning light greatly affect a measurement's outcome (Figure 2.6). Reducing the light's time (or spatial) coherence results in higher measurement resolution. Low/Partial Coherence Interferometry (LCI/PCI) is a type of interferometry that relies on this property. However, while temporal coherence affects axial resolution, spatial coherence affects lateral and axial resolution. Early work in LCI showed contrast degradation in result of low spatial coherence [5]. Therefore, low time coherence light is used in PCI.

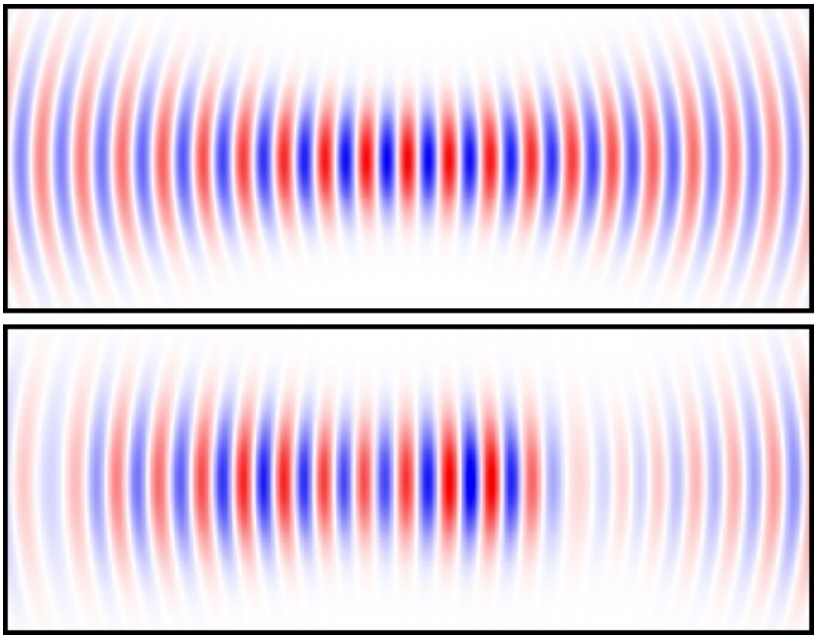

Figure 2.6: Electric field distribution around the focus of a Gaussian laser beam. Upper image: perfect spatial and time coherence; Lower image: high spatial coherence, poor time coherence.

Axial resolution is defined by the coherence length of a light source. Its lateral resolution depends on the optics used to focus the probe beam onto the sample. A light source's coherence length, l_c, is defined according to the following equation:

$$l_c = \frac{\lambda_0^2}{\Delta\lambda} \tag{2.1}$$

where λ_0 is the source's mean wavelength and $\Delta\lambda$ its spectrum wavelength width (FWHM).

Interferometry using coherent light shows interference patterns for distances multiple of coherence wavelength. Using light with low time domain coherence, interference is only detected for waves with path difference smaller than the coherence length of the light, allowing greater measurement resolution and precision[10].

While a conventional Michelson interferometer set-up is sensitive to longitudinal object movements, introducing a second interferometer arm (a so-called dual beam set-up - Figure 2.7) allows total independence from longitudinal movements. A reference structure within the object is used as reference in order to neglect these movements. Therefore, dual-beam interferometry is used in systems that are prone to unavoidable movement and are intrinsically non-static.

Inside the AC Master (Figure 2.7), some parameters of a laser diode are used as light source (LS) in a Michelson interferometer setup [15]. This infra-red beam, with high spatial coherence but very short coherence length, is then split into two components, forming a coaxial dual beam. This dual light beam contains two beam components with a mutual time delay of twice the interferometer arm length difference, 2d, introduced by the interferometer (making this a time domain system). It illuminates the eye, and both components are reflected at several intraocular interfaces.

An interference signal only occurs if the delay of these two light beam components equals an intraocular distance within the coherence length of the light source. This results in measurements with very high axial resolution (12 μm) and detection precision (.3 to 10 μm)[9],[10],[22].

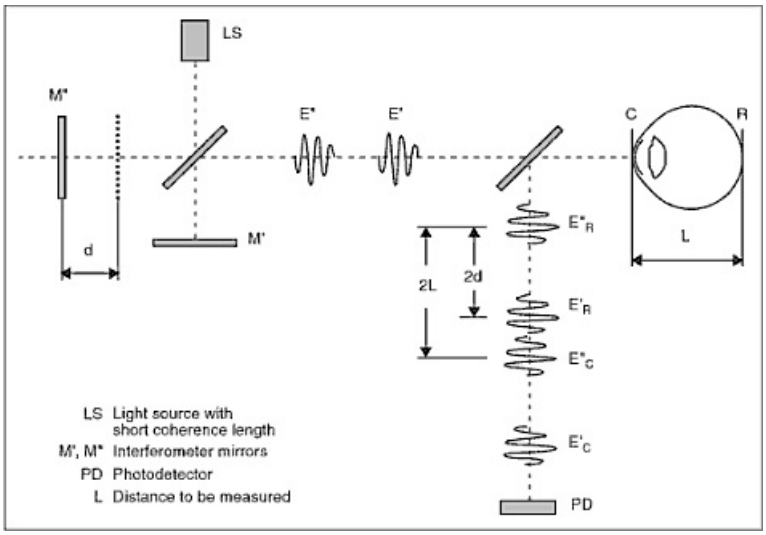

Figure 2.7: Basic set-up of a dual beam partial coherence interferometer. From [15].

An example of the AC Master's final measurements are shown in Figure 2.8. A depth scan is performed along the eye's aligned axes (optical and visual) and interferometry peaks occur whenever the scanning depth matches an interface distance within the eye.

The resulting interference signal in the AC Master is a probing depth vs. relative intensity graphic. Intensity peaks exist whenever an interface is detected along the scanning depth. Lower intensity peaks may also arise from autocorrelation of the strong signal. Figure 2.8 shows such a measurement example. In this graphic, the AC Master automatically indicates the most probable corneal and lens interface peaks:

- ACS - anterior corneal surface;
- PCS - posterior corneal surface;
- ALS - anterior lens surface;
- PLS - posterior lens surface.

Therefore, anterior chamber depth (ACD) is calculated as the xx' axis value distance between peaks PCS and ALS.

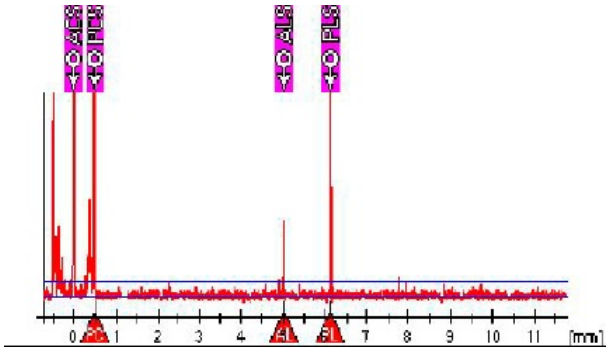

Figure 2.8: Measurement example. From [22].

2.5 Project Overview

This project's main goal is to investigate a novel more user friendly approach to perform accurate anterior chamber depth (ACD) interferometry measurements. Perfect alignment between the eye's optical axis and its visual axis is of greatest practical importance, since precise measurements can only be acquired in such conditions. This new approach will rely on having the subject focus on a moving target instead of a fixed one.

Previously, the subject was asked to focus his gaze on a fixed target - a lit pixel on the AC Master's internal OLED. The light coming from this pixel would reflect on the eye's optical surfaces and create the desired Purkinje reflections. The technician would then adjust the instrument's position (using the joystick) in order to make the Purkinje reflections overlap [22], meaning that the eye's optical axis is aligned with the measurement beam.

Accommodation of the patient, involuntary eye movements, natural lens tilting and technician's inexperience would make overlapping the reflections very difficult.

A different method was devised in order to improve measurement conditions. Instead of having the subject focus on a fixed target, the patient is asked to focus on a target as it moves.

A pixel is lit for a fixed time, then another is lit while the previous is turned off. In this way, the subject sees the target moving. Therefore, the eye's optical axis changes orientation as the target moves, changing the Purkinje reflection's relative positions. This method would eliminate accommodation difficulties that previously existed from focusing on a fixed target. The pixel illumination sequence is programmed to form a spiral pattern (see section 3.3).

The CCD camera sends live Purkinje reflections video to the computer. The video's image sequence is then subject to image analysis in order to differentiate the reflections. The main goal would be to detect the third Purkinje reflection in every image, therefore following its movement. Whenever the third reflection is detected overlapping the first one, the OLED's lit pixel position should be recorded as a good measurement position.

If, however, no overlapping is detected in the considered sequence, this approach is not useful. A new method was devised in order to calculate an adequate measurement position in case overlapping is not detected.

The proposed method is based on creating a model for the third Purkinje reflection's movement as the eye tilts. Even when no overlapping is detected, if still some third Purkinje reflections can be detected throughout the target's movement, then a feasible approach is to use this model to extrapolate an adequate target location that brings both reflections into an overlapping position. Since for a certain degree of eye tilt the third Purkinje reflection is no longer seen, programming the target's movement can take this into account, allowing to further limit its movement amplitude. This method is described in detail in Section 3.5.

2.6 State of the Art

There are currently three main technologies in ACD measurements: interferometry-based instruments (which is the AC Master's category), ultrasound-based measurements and Scheimpflug principle-based imaging. The first two technologies are very closely related, given that both work on the basis of detecting waves that reflect off of boundary surfaces. Ultrasound biometry uses sound waves, whereas interferometry employs infra-red light. The latter relies on an optical imaging planes intersection principle, referred to as the Scheimpflug principle (which will be further explained in the following section).

2.6.1 Wave Interference Technology

Prior to interferometry-based measurements, A-scan ultrasound measurements were routine in biometry measurements for precise IOL refractive power calculations in cataract surgery [10].

In order to perform ultrasound measurements of the sampled object, as in any other ultrasound-based medical examination, there must be direct contact between the transducer and the object. Additionally, a transmitting gel has to be used in order to avoid transmission dampening.

These particular set-up requirements imply some procedural disadvantages [2]: first of all, anaesthesia is required for the procedure to be undertaken (see Figure 2.9); transducer contact pressure on the eye can change eyeball shape consequently affecting measurement outcome; contact with gel may give rise to infections. On the other hand, some advantages of ultrasound measurements bring forth some advantages: patient cooperation is required to a lesser extent; this procedure can be used for mature cataracts (dense media).

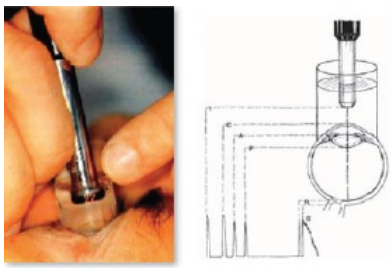

Figure 2.9: Ultrasound biometry procedure set-up. From [2].

A comparison regarding resolution and precision between both technologies is also required, as is the effective outcome on IOL power calculations.

At 10MHz, the longitudinal resolution of an ultrasound transducer is approximately 200 μm, whereas the resolution of interferometry is aprroximately 12 μm, with precision less than 10μm [10] (as mentioned previously). Ultrasound biometry errors have been shown to be responsible for 54% of predicted refraction errors, resulting in a postoperative IOL refractive error of 0,28 diopters [1],[10].

Some disadvantages of interferometry procedure include [2]: great extent of patient cooperation required (patient needs to fixate on a target); cannot be used for mature cataracts; and, of course, procedural difficulties arise because of the need to align the eye's optical and visual axes (which is the main concern of this project).

2.6.2 Scheimpflug-based Imaging

An alternative to wave interference technology, requiring less patient cooperation, is Scheimpflug-based imaging. The Scheimpflug principle states that when the lens plane (LP) and the image plane (IP) of an optical system are not parallel (there is an inclination between both other than 180Âº), the plane of focus (PoF) is unique and such that all three planes (LP, IP and PoF) meet alongs a single line, called the Scheimpflug line (see Figure 2.10).

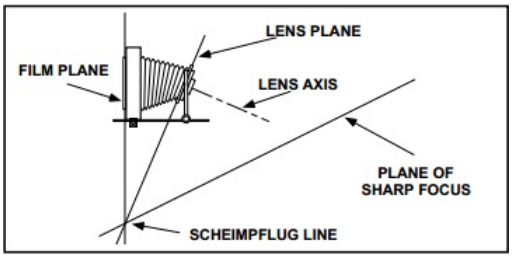

Figure 2.10: Scheimpflug principle. From [17].

A Scheimpflug-based imaging technique uses a tilted camera whose PoF is a plane that crosses the eye at an oblique angle, obtaining images that show cross-sections of all structures of the eye up to posterior lens surface depth [13],[16] (see Figure 2.11(a)). Taking images around the eye allows cross-sectional views of the entire anterior chamber. These images are then analysed for tissue boundaries and finally topography images of the cornea is generated, along with determination of ACD.

This technique is an alternative to wave front technologies. This method has the disadvantages of limiting its use for eyes free of light-scattering sources, i.e., opacities, scarring, deposits or edema. Studies show, however, that measurement errors are within the same range as for ultrasound and interferometry measurements [16].

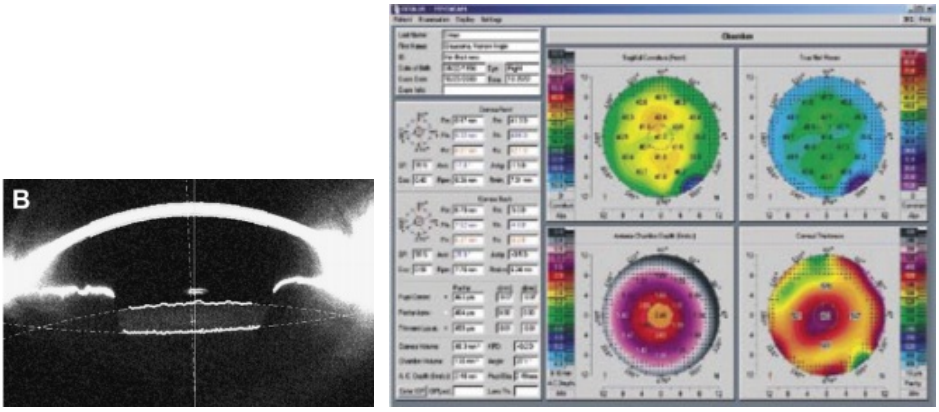

(a) Example of a Scheimpflug image, showing a cross-section of the eye (from cornea to posterior lens surface). From [3].

(b) Example of Scheimpflug-imaging corneal plots. These plots show corneal density and topography. From [13].

Figure 2.11: Scheimpflug-based imaging.

3. Materials and Methods

3.1 Introduction

A complete procedure to capture and analyse Purkinje reflections and ultimately estimate each subject's correct target positioning is explained in this section. The complete procedure should follow the following guidelines:

1. Patient's eye should be properly aligned with the instrument;
2. Patient will follow a focusing target in the instrument in order to make the Purkinje reflections move; all the while this movement is being recorded;
3. Recorded images are analysed in search for third Purkinje reflection;
4. Results from image analysis are used to estimate correct target positioning.

The AC Master from Zeiss Meditec, AG was used in these experiments. Labview software is used to model the target's positioning and movement in the instrument's internal OLED, as well as retrieving and recording videos and images of the resulting Purkinje reflections.

3.2 Aligning Subject and Instrument for Image Capturing

There are two main steps in properly aligning the subject's optical axis with the instrument's beam:

I. Coarse alignment of the eye with the instrument's beam;

II. Fine alignment, with the help of Purkinje reflections.

The following described procedure will hold valid for any alignment made for a test eye (as in Section 3.5.2).

I. **Coarse Eye and Instrument Alignment**

The subject's eye has to be aligned with the Exit Aperture of the Super Luminescent Diode (Figure 2.3).

(I.1) Subject places his chin and rests his forehead on the chin and forehead rests (Figure 2.5). Subject should be comfortably seated, so that his breathing and other body movements won't make his eye move in the operator's view.

(I.2) Meanwhile, operator turns equipment on. Creates new patient profile (Name, Date of Birth), or accesses an existing one.

(I.3) Measurement mode is automatically initiated after patient profile step is completed. Operator should choose either White to White (WtW) or Pachymeter measurement mode (Figure 3.1, Table 2.1), where live video is shown. Changing between modes is done pressing Tab on keyboard until desired mode is chosen.

(I.4) Operator adjusts eye height relative to Exit Aperture of SLD through rotation of vertical headrest control (Figure 2.5), in order to fully frame the eye inside the live video image.

(I.5) Patient sees yellow fixation target and is asked to focus on it.

(I.6) Align illumination LEDs (reflected in the cornea) with pupil (Figure 3.2). Move joystick forward/backwards slightly beyond focus point (when illumination LEDs are slightly enlarged after being perfectly focused).

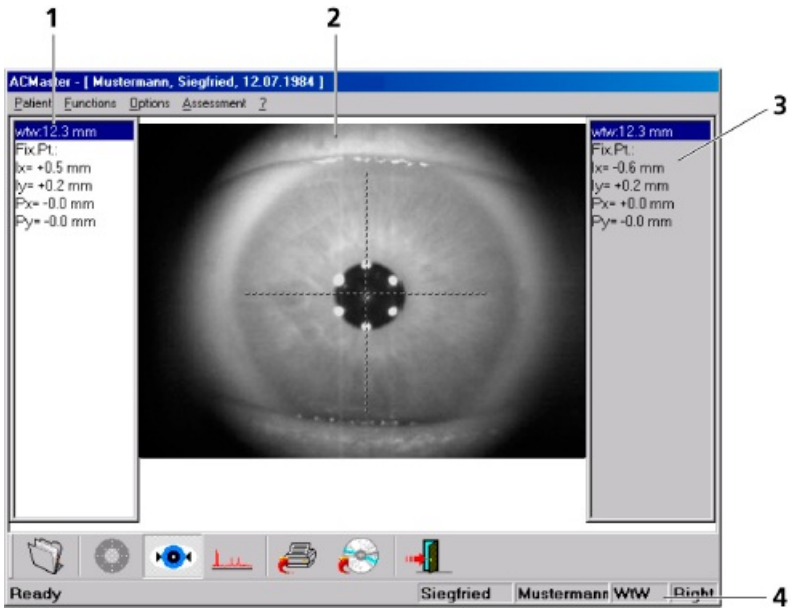

Figure 3.1: WtW measurement mode screen: 1 - Display field for results of right eye; 2 - Live video image; 3 - Display field for results of left eye; 4 - Status, first name, name, measuring mode and eye (right/left) of live image. From [22].

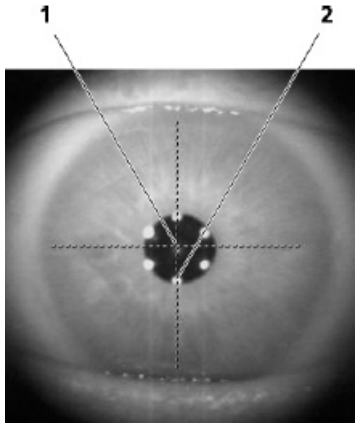

Figure 3.2: WtW alignment: 1 - Image of fixation point; 2 - Image of illumination LED (reflection point). From [22].

I. **Fine alignment Using Purkinje Reflections**

The operator should now align the subject's optical axis with the instrument's beam.

(I.1) Change to ACD measurement mode. The operator will now observe the first Purkinje reflection and look for the third one (in case it isn't immediately visible) by moving the joystick. Doing so, he will also align them as best as possible.

(I.2) There should be no forward/backwards movement of the joystick, which would change the previously obtained focus point.

(I.3) Rotating the joystick over itself will move the third Purkinje image closer/further away from the first Purkinje image.

(I.4) Moving the joystick left/right will move the third Purkinje image horizontally.

(I.5) The third Purkinje image should be overlapping the first Purkinje image perfectly.

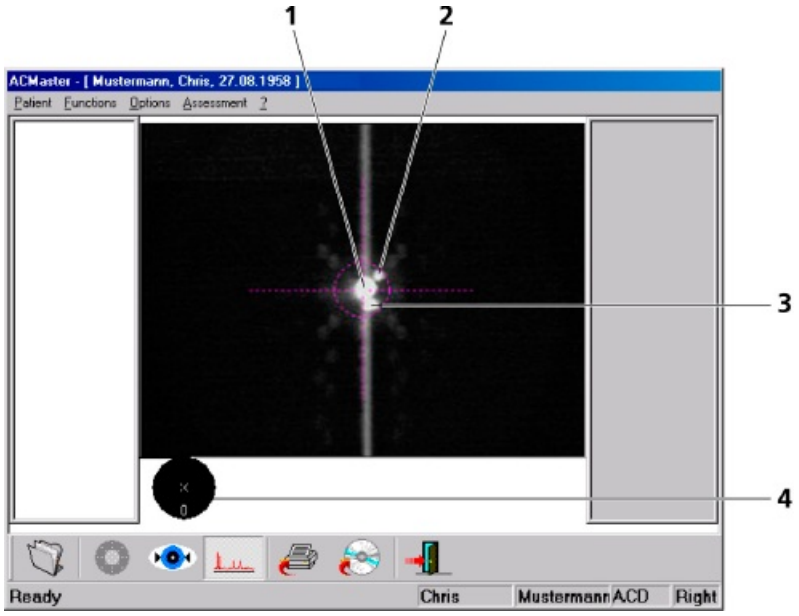

Figure 3.3: ACD measurement mode, for Purkinje reflections alignment: 1 - Reflection from anterior corneal surface; 2 - Reflection from posterior lens surface; 3 - Reflection from anterior lens surface; 4 - Position of fixation target on internal LC display. From [22].

3.3 Capturing Images for Analysis

After aligning subject and instrument, the subject will follow a fixation target programmed through a Labview interface. This interface also allows simultaneous recording of the resulting Purkinje reflections.

3.3.1 Following the Fixation Target Pattern

The subject must focus on a target that he sees as he looks into the exit aperture. The target is a 3 RGB coloured pixel on the OLED. It changes position according to a previously programmed pattern and the subject should follow it. As the eye moves, so do the Purkinje reflections, eventually overlapping.

The target's movement pattern and speed is programmed in the Labview interface, in order to meet optimal criteria for each patient. It consists of a series of circular loops, starting from the center and going outwards. The loop's center is the previously determined alignment spot.

Several parameters are programmable, such as the number of loops and position changing speed (how long the pixel remains lit after changing position), etc.

Some scanned portions of the spiral will yield no third Purkinje reflections for a certain subject, whether others are highly dense with reflections. Therefore, a further useful feature allows cropping the target's complete circular moving pattern into smaller loop quadrants or sections (Figure 3.4(b)) where there is a higher third Purkinje reflections occurrence.

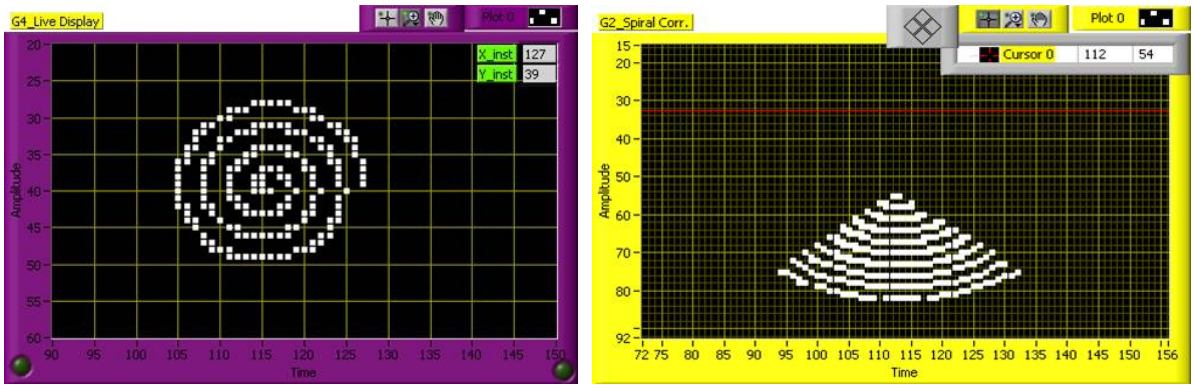

(a) Full spiral, 4 loops.

(b) Spiral section, 10 loops.

Figure 3.4: Programmed target shape.

3.3.2 Image Capturing

Initially, the CCD camera was accessed for video capturing. It was manually enabled and stopped, before starting target movement and after the target finished its programmed path, respectively. This yielded a video containing the Purkinje reflections' movement as the target followed its path, but also a set of frames prior and after target movement where no target movement happened.

Capturing video in this way did not allow straightforward time correlation between video and programmed target position, since there was no accurate way of knowing which video frame corresponded to the first target position.

Having a good time correlation between video frame and target position is crucial in order to achieve accurate automatic target positioning extrapolation (section 3.5). Therefore, instead of capturing a whole video during each experience, the computer saves the CCD camera image at each instant of target position change.

Additionally, a string array stamp was added to the image, saving the image under that same name. The string contains a time stamp and the target's X and Y position at that instant. This way, when accessing an image for image analysis, the target's position at that instant is also known.

Figure 3.5: Example of captured image.

3.4 Image Analysis

3.4.1 Image Features

In order to detect the third Purkinje reflection on the recorded images, a series of image features need to be ignored. To understand the chosen method, an introduction of what can be seen in every image and also how it changes from image to image is given.

3.4.1.1 Static

Every captured image is of type double and 480 x 640 pixels, with pixel intensity range [0-255]. The third Purkinje reflection is not present in all images. Some features that appear in every image and must be taken into account while performing image analysis are (Figure 3.6):

- The first Purkinje reflection (1P);
- a white column directly in the middle of the image, resulting from sensor saturation of the CCD camera (C).

There are also artefacts that appear and clearly are not third Purkinje reflections (Figure 3.8). They include:

- A matrix-shaped set of white spots (MS), which are the images of LED's array in the OLED;
- a halo (H) surrounding the first Purkinje reflection;
- an elongated elliptical shape (ES);
- a non circular 1P, resulting from optical axis and illumination beam getting out of alignment. A scattered trail of light (TL) accompanies this effect, protruding from 1P. In this situation, sometimes even 3P is present. ES can also appear.

(a) Original image.

(b) Artefacts highlighted: 1P - first Purkinje reflection; 3P - third Purkinje reflection; MS - matrix-shaped set of spots; H - halo; C - white column.

Figure 3.6: Most common artefacts.

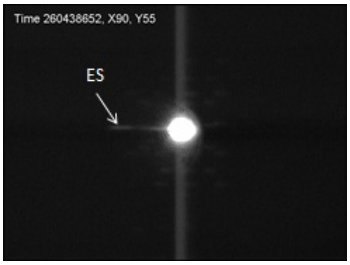

Figure 3.7: Sporadic artefacts.

(a) Trail of light (TL) can be seen. Elongated elliptical shape (ES) also present.

(b) TL present. Third Purkinje (3P) also present.

Figure 3.8: Artefacts resulting from misalignment.

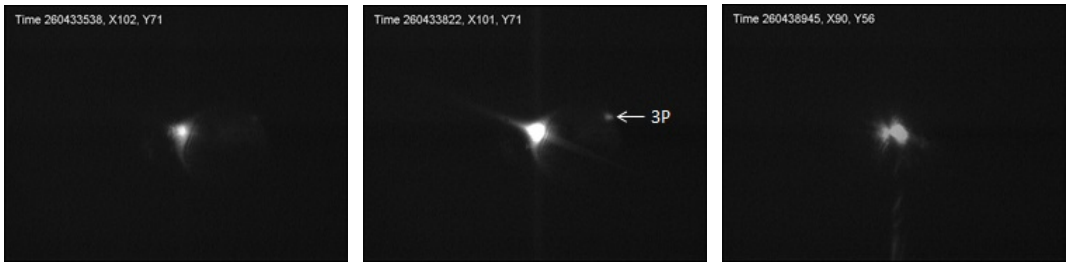

(a) An example of misalignment. 1P is very distorted.

(b) An example of misalignment. 1P is very distorted. 3P is also visible.

(c) An example of misalignment. 1P is very distorted.

Figure 3.9: Misalignment examples.

3.4.1.2 Motion-related Features

The third Purkinje reflection can be seen changing position along a set of images. It can be absent on an image and appear on the next one (Figure 3.10).

Although it follows a somewhat circular movement pattern in agreement with the moving target, its speed is not constant and can often disappear due to extreme tilting of the eye. Its shape and size often change, overlapping with the white vertical column and other artefacts is common, giving rise to many movement inconsistencies.

Other artefacts also move and change shape, its position change being sometimes more noticeable than the third Purkinje reflection's. The elongated shape (Figure 3.7) changes shape dramatically very randomly, and the white vertical column can be seen moving from side to side.

In conclusion, there are many objects within the images whose shape, size and position change just as often as the third Purkinje reflection's. Furthermore, the rate at which these changes occur is not constant. The result is that relying on its movement to detect the third Purkinje reflection will turn out to be very difficult (4.1.2).

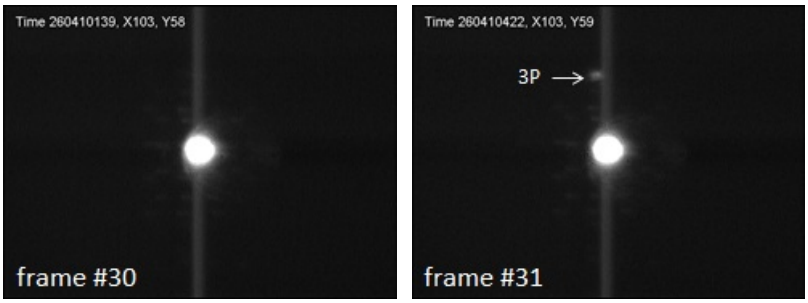

(a) Frame # 30. No 3P is visible.

(b) Frame # 31. 3P visible.

Figure 3.10: 3P appearing within consecutive frames.

3.4.2 Final Procedure

An algorithm based on pixel intensity differentiation, connected components size and relative location was ultimately used. This section describes it in more detail.

I. **Stored image is read.**

   At the same time its top is cut off, so that the time and target position stamp is removed, so as to not interfere in pixel intensity differentiation.

II. **Coarse pixel differentiation - separating first and third Purkinje reflections.**

   The first Purkinje reflection can be easily separated by keeping only the highest intensity pixels. This image will be called *first Purkinje image*.

   Performing dynamic thresholding on remaining pixels allows better differentiation of lower intensity pixels. This image will be referred to as *third Purkinje image*.

III. **Isolate first Purkinje reflection.**

   Since later on we need to detect the location of both first and third Purkinje reflections, we must make sure that there is only one connected object in previously created *first Purkinje image*. Therefore, only the largest connected component is kept.

IV. **Cropping within area of interest.**

   One step that can be taken in order to reduce incorrect detection of third Purkinje reflections is to narrow down the search area.

   Taking *first Purkinje image* (currently only showing the first Purkinje reflection), create a cropping window centred in first Purkinje reflection, with 280 pixel x 280 pixel size.

   Crop *third Purkinje image* according to this cropping window. This reduces detection of non-third Purkinje reflection pixels that appear farther away from where the third reflection could ever be seen.

V. **Detecting third Purkinje reflection.**

   Taking the now cropped *third Purkinje image*, make sure only one connected component is detected.

   Every connected object with size larger than a normal first Purkinje reflection is removed. Erosion and dilation is performed to gradually remove small objects. If there are still more than one object detected, remove objects formed by less than 120 pixels.

VI. **Final third Purkinje detection criteria.**

   If the detected third Purkinje object's is horizontally too close to the first Purkinje object, don't use it.

   This step discards all detected pieces of the vertical stripe in the original image.

3.5 Automatic Target Positioning

An ultimate goal of this project is to calculate where the target should be positioned in order to achieve perfect overlapping of the first and third Purkinje reflections. When no overlapping is detected through image analysis, the relationship between third Purkinje reflection movement as the eye rotates while following the target must be known.

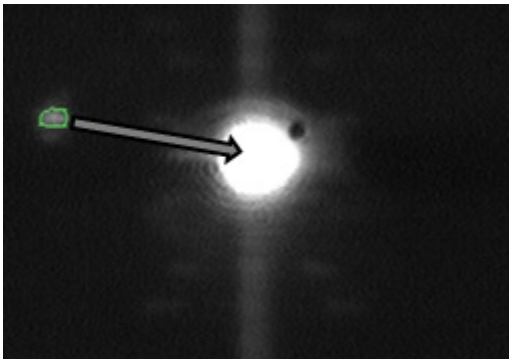

Figure 3.11: Procedure to make detected third Purkinje reflection (green outline) follow arrow's path, so that it overlaps first Purkinje reflection

The subject focuses his eye on a target which is a light spot in the OLED inside the AC Master. As the spot moves, the eye follows it and there's a corresponding movement of the Purkinje reflections.

A known feature of the OLED inside the AC Master is that it is not fitted perfectly straight. The display is rotated, resulting in a rotation of the target's movement from the originally programmed. Furthermore, one must know how the third Purkinje reflection moves as the eye moves. Therefore, there are at least two variables one must take into account when calculating where to place the target in order to make the third Purkinje reflection overlap the first one (Figure 3.11). These relationships have to be determined in order to know how the Purkinje reflections relate to the target's movement (Figure 3.12).

Two experiments were set up in order to calculate the OLED's rotation inside the AC Master and how the third Purkinje reflection moves as the eye moves.

A third experiment was also performed, in order to determine the error associated with the third Purkinje reflection's location.

They are described in the following sections.

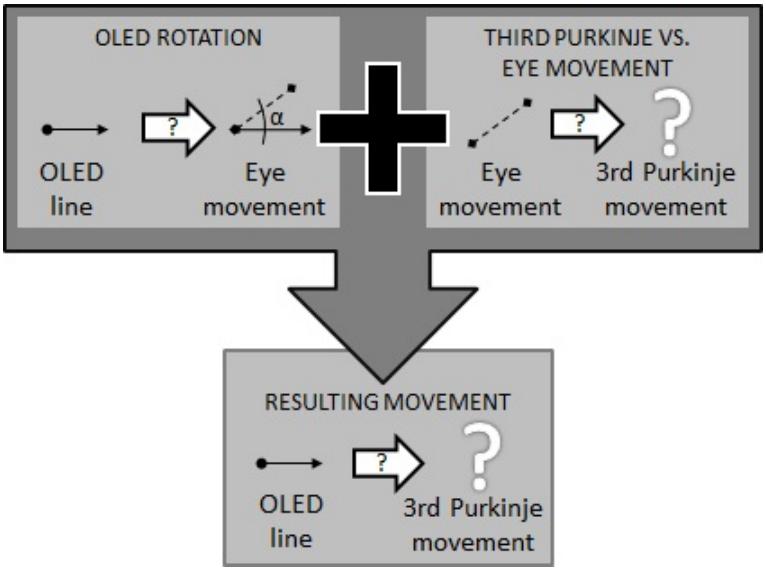

Figure 3.12: Dependencies between movements in predicting third Purkinje reflection movement.

3.5.1 OLED Rotation

3.5.1.1 Measurements

Instead of programming a single spot in the OLED, a line segment was programed in Labview to appear in the OLED (Figure 3.13). Two points are programmed as endpoints of that line segment (X1, Y1 - left; X2, Y2 - right). The right endpoint is fixed, the left one moves with arrow keys keystrokes on the AC Master keyboard.

1. With the AC Master already turned on and communicating with the computer, run program on Labview that makes a line segment appear in the OLED (Figure 3.13).
2. Subject should place his head and chin comfortably on chin and headrests of the AC Master (Figure 2.5).
3. Subject should adjust eye height with vertical head rest control (Figure 2.5) in order to perfectly see line segment inside the AC Master.
4. Subject should use arrow keys on AC Master's keyboard to move left extremity and make line segment as horizontal as possible.
5. Record coordinates of X1, Y1 point.
6. Repeat for several subjects.

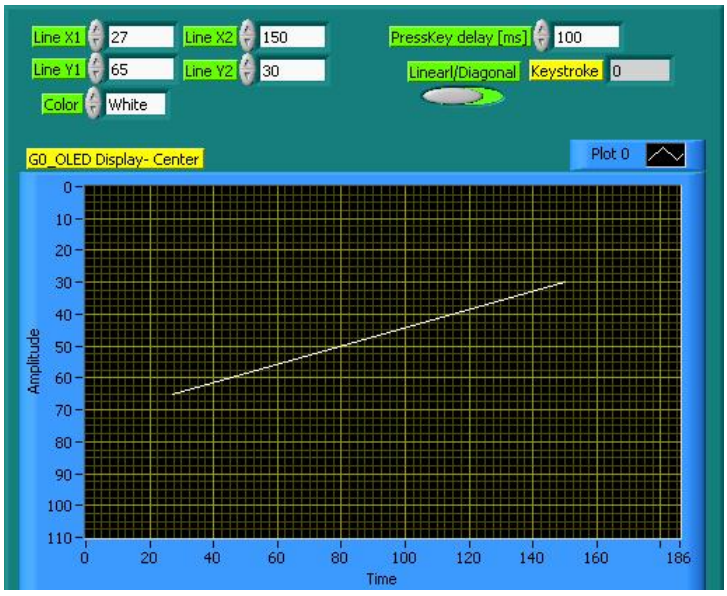

Figure 3.13: Programmed line in Labview to test OLED rotation.

3.5.1.2 Data Analysis

Figure 3.14 depicts the scheme to calculate the OLED rotation inside the AC Master. When the line is in the final position, the subject sees a horizontal line in the AC Master's OLED. Results and final calculations in section 5.2.1.

$$\begin{aligned} \cos\phi &= \frac{|FinalPosition|}{|StartingPosition|} \\ &= \frac{\sqrt{(X_{1,last} - X_{2,first})^2 + (Y_{1,last} - Y_{2,first})^2}}{\sqrt{(X_{1,first} - X_{2,first})^2 + (Y_{1,first} - Y_{2,first})^2}} \end{aligned} \tag{3.1}$$

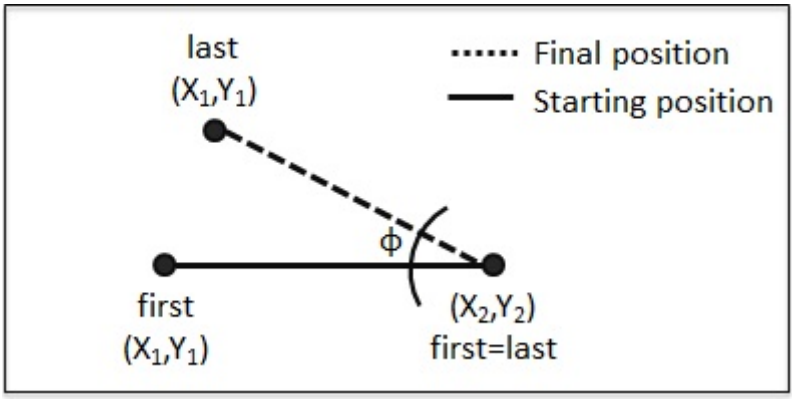

Figure 3.14: Programmed line's starting and final positions for OLED rotation calculation.

3.5.2 Purkinje Reflections Separation vs. Eye Tilt

A test eye [1] attached to a goniometer (Figure 3.15) was mounted on its corresponding mounting spots in the AC Master's headrest (Figure 2.5,5), to study the third Purkinje reflection's as the eye tilts.

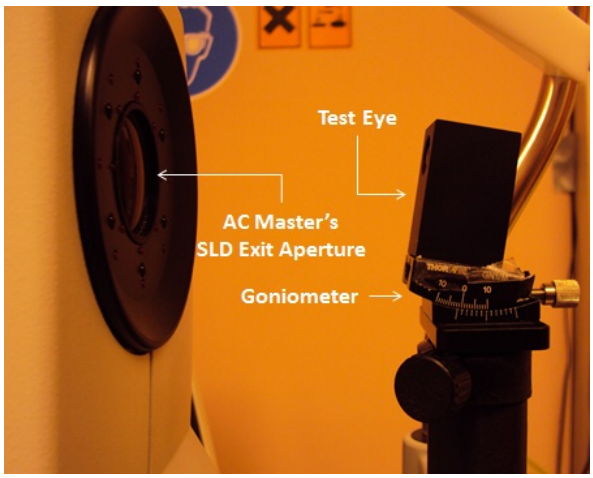

Figure 3.15: Test eye and goniometer mounted in the AC Master for eye tilt measurements.

3.5.2.1 Measurements

I. **Setting Up the System**

(I.1) With the AC Master already turned on and communicating with the computer, run video capturing program that will show CCD camera live video (the same that is seen in the AC Master's external OLED, Figure 2.3,2).

(I.2) Mount test eye in the AC Master (Figure 2.5,5). Be sure that eye side is as parallel to mounting beam as possible, which will help with initial test eye alignment. Also make sure that the goniometer reads 0°.

(I.3) Adjust vertical head rest control (Figure 2.5), placing test eye as close to Exit Aperture of SLD (Figure 2.5) as possible.

(I.4) Now the test eye should be aligned with the measurement beam, in the same way done in section 3.2.

(I.5) Once it is correctly aligned, this alignment can be checked. Still in ACD measurement mode, use the interferometry measurement button to check if a good measurement is done. This ensures that there is an adequate alignment between the test eye's optical axis and the measurement beam.

[1] A test eye is an optical testing device with two built-in lenses mimicking the human eye's cornea and lens.

II. **Tilting and Recording Measurements**

(II.1) Using the goniometer handle, tilt the eye in small steps. Take a snapshot of the captured video (Figure 3.16(a)), for further image analysis to calculate distance between first and third Purkinje reflections.

(II.2) Repeat tilting and taking snapshots, until reaching tilt where third Purkinje reflection is no longer visible.

(II.3) Once the reflection has disappeared, continue tilting the eye in the opposite direction and taking snapshots at each tilt.

(II.4) With this procedure, both directions of the tilting axis are scanned (Figure 3.16(b)).

3.5.2.2 Data Analysis

Since the measurable angle range was very small and the goniometer scale too large for the performed tilts, it was not possible to record the angle where each snapshot was taken. Instead, recording maximum and minimum angles was the devised method. This way, taking the number of snapshots between these extremities, a rough angle step estimation can be calculated.

Therefore, let θ_1 and θ_2 be extremities angles, s_1 and s_2 be first and last snapshot. The angle step, θ_{step}, is thus

$$\begin{aligned} \theta_{step} &= \frac{\Delta\theta}{\Delta s} \\ &= \frac{\theta_2 - \theta_1}{s_2 - s_1} \end{aligned} \tag{3.2}$$

Image analysis on these images was performed simply by detecting highest intensity pixels, after performing Otsu's threshold. Since the test eye is made with glass lenses, there are less artefacts present than in a normal human eye would be. Both the first and third Purkinje reflections were regions of very high intensity pixels, enabling a very straightforward detection procedure.

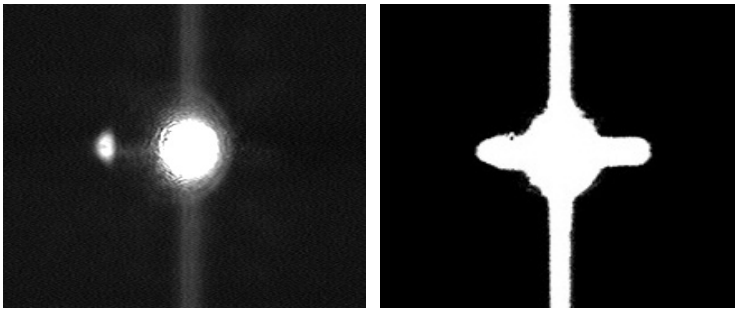

(a) Example of a snapshot. (b) Resulting horizontal movement.

Figure 3.16: Measuring test eye tilt.

Calculations and results from these experiments presented in section 5.2.2.

3.5.3 Eye Fixation Deviation

A subject stared at a fixed target in the AC Master's OLED for some time, and a video was recorded. This video was then subject to image analysis to detect the third Purkinje reflection. In this way, we can see how precise is the location of the third Purkinje reflection when looking at a target. Figure 5.2.3 shows how the third Purkinje reflection moves even when the eye is fixating a target.

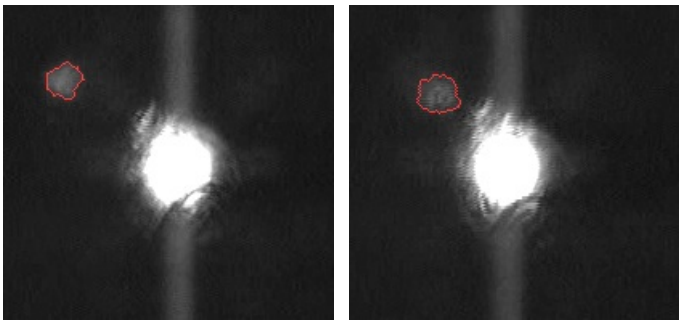

(a) Detected third Purkinje farther away from first Purkinje.

(b) Detected third Purkinje closer from first Purkinje.

Figure 3.17: Third Purkinje location changes with fixed target.

Results from this experiment are shown in section 5.2.3 and further discussed in Chapter 6.

3.5.4 Final Calculations

For each pair of detected third Purkinje reflections and corresponding detected first Purkinje reflections, their

Therefore, given two images, k_1 and k_2, where third Purkinje reflections were detected, let:

- $\vec{d}_j$ be the displacement vector of either programmed target (pt), OLED pixel (Op), first or third Purkinje reflection (1P, 3P) ($j = \{pt; Op; 1P; 3P\}$);
- $x_{j,k}$ and $y_{j,k}$ be j's x and y coordinates on image i ($k = \{k1; k2\}$);
- ϕ be the calculated OLED rotation (from section 3.5.1);

The goal of the following equations is to find the relation between the tilt of the eye (which is to say, its visual and optical axis) and the corresponding displacement of the fixation target in the OLED.

Vector $\vec{d_{Op}}$ is a rotation of vector $\vec{d_{pt}}$, given that the OLED is rotated ϕ degrees inside the AC Master. It is assumed that no shrinkage or expansion occurs. Therefore, in complex space, we have,

$$\vec{d_{Op}} = \vec{d_{pt}} \cdot \exp(\phi i) \tag{3.3}$$

as seen in Figure 3.18(a).

On the other hand, having studied third Purkinje reflection's movements as the eye rotates, we know that its displacement vector must be a function of the OLED pixel's displacement. It was shown that this is a linear relation (section Results and Discussion). Therefore,

$$\vec{d_{3P}} = \beta \cdot \vec{d_{Op}} \tag{3.4}$$

as seen in Figure 3.18(b).

Combining both equations (3.3 and 3.4), we have the relationship between third Purkinje reflection and programmed target to be,

$$\vec{d_{3P}} = \beta \cdot \vec{d_{pt}} \cdot \exp(\phi i) \tag{3.5}$$

as seen in Figure 3.19.

Given that the angle change occurs due to Labview-OLED transformation, we take that β can be calculated as follows,

$$|\vec{d_{3P}}| = \beta \cdot |\vec{d_{pt}}| \tag{3.6}$$

Therefore, knowing the programmed target's and third Purkinje reflection's coordinates on both images, we have,

$$\begin{cases} |\vec{d_{3P}}| = \sqrt{(x_{3P,k2} - x_{3P,k1})^2 + (y_{3P,k2} - y_{3P,k1})^2} \\ |\vec{d_{pt}}| = \sqrt{(x_{pt,k2} - x_{pt,k1})^2 + (y_{pt,k2} - y_{pt,k1})^2} \\ \beta = \frac{|\vec{d_{3P}}|}{|\vec{d_{pt}}|} \end{cases} \tag{3.7}$$

On the other hand, in cartesian space, the third Purkinje reflection's and target movement's equations are as follows,

$$\begin{cases} x_{3P,k2} = x_{3P,k1} + \Delta x_{3P} \\ y_{3P,k2} = y_{3P,k1} + \Delta y_{3P} \\ X_{pt,k2} = X_{pt,k1} + \Delta X_{pt} \\ Y_{pt,k2} = Y_{pt,k1} + \Delta Y_{pt} \end{cases} \tag{3.8}$$

Accordingly, in cartesian space, equations 3.3 and 3.4 can be written as,

$$\begin{cases} \Delta x_{pt} = \Delta x_{Op} \cdot \cos\phi \\ \Delta y_{pt} = \Delta y_{Op} \cdot \sin\phi \end{cases} \tag{3.9}$$

and,

$$\begin{cases} \Delta x_{3P} = \Delta x_{Op} \cdot \beta \\ \Delta y_{3P} = \Delta y_{Op} \cdot \beta \end{cases} \tag{3.10}$$

again, assuming a linear relation between OLED pixel's movement and third Purkinje reflection's movement (no rotation).

Taking equations 3.9 and 3.10, and solving it for Δx_{pt} and Δy_{pt}, we have,

$$\begin{cases} \Delta x_{pt} = \Delta x_{3P} \cdot \frac{\cos\phi}{\beta} \\ \Delta y_{pt} = \Delta y_{3P} \cdot \frac{\sin\phi}{\beta} \end{cases} \tag{3.11}$$

On the other hand, the third Purkinje reflection's final position must match the first Purkinje reflection's position. It is also assumed that the first Purkinje reflection doesn't move. Taking also 3.11 into 3.8, we have,

$$\begin{cases} \Delta x_{3P} = x_{3P,k1} - x_{1P} \\ \Delta y_{3P} = y_{3P,k1} - y_{1P} \\ x_{pt,new} = x_{pt,k1} + \Delta x_{3P} \cdot \frac{\cos\phi}{\beta} \\ y_{pt,new} = y_{pt,k1} + \Delta y_{3P} \cdot \frac{\sin\phi}{\beta} \end{cases} \tag{3.12}$$

In conclusion, in order to estimate new target coordinates ($x_{pt,new}$,$y_{pt,new}$) for better alignment, we have,

$$\begin{cases} x_{pt,new} = x_{pt,k1} - (x_{1P} - x_{3P,k1}) \cdot \frac{\cos\phi}{\beta} \\ y_{pt,new} = y_{pt,k1} - (y_{1P} - y_{3P,k1}) \cdot \frac{\sin\phi}{\beta} \end{cases} \tag{3.13}$$

where β is given by equation 3.7.

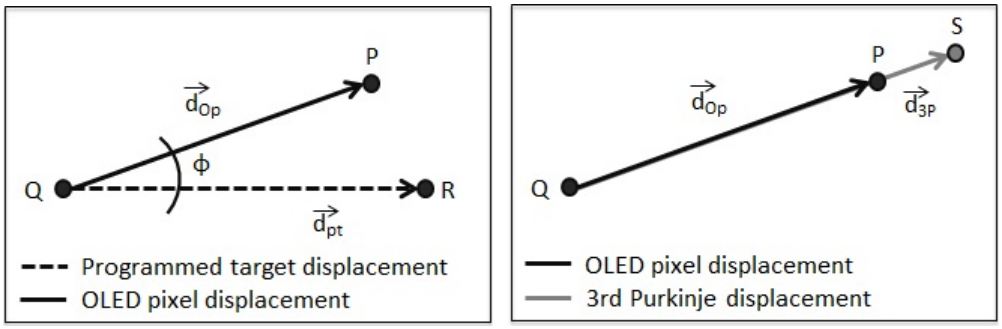

(a) Rotating $\vec{d_{pt}}$ by ϕ gives $\vec{d_{Op}}$. (b) Scaling $\vec{d_{Op}}$ by β gives $\vec{d_{3P}}$.

Figure 3.18: Transforming $\vec{d_{pt}}$ into $\vec{d_{Op}}$, and $\vec{d_{Op}}$ into $\vec{d_{3P}}$.

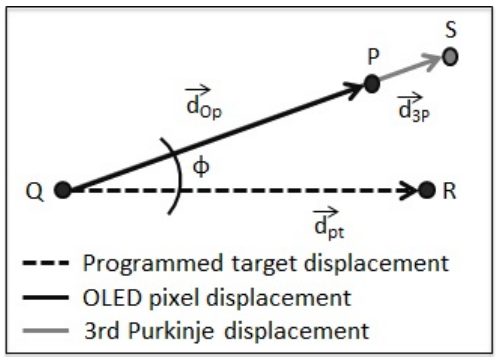

Figure 3.19: $\vec{d_{pt}}$ gives $\vec{d_{3P}}$ through rotation by ϕ and scaling by β.

4. Related Work

Working on how to detect the third Purkinje reflection was the most time consuming step of the project. The results of this research ultimately changed this project's approach to achieve optical axis and measurement beam alignment. Chapter 3 already presented the final chosen approach, therefore this chapter will comprise a summary of tested image analysis approaches that proved ineffective.

Since these approaches were not ultimately used, a short discussion on their results and effectiveness within this project's framework is also presented in this chapter, rather than being dispersed in chapters 5 and 6, which are dedicated only to actually used approaches.

4.1 Searching for an Optimal Image Analysis Procedure

The first step every image analysis algorithm should undergo is applying adequate image threshold. Reducing image noise level improves the chances to detect meaningful regions within the image.

Differentiation of regions within the image, however, can be achieved through a multitude of methods. In this project, the main tested approaches dealt with frame differentiation and shape differentiation.

4.1.1 Pre-Analysis

Thresholding the recorded images is the first step to be taken.

Every picture had a slightly different gray value histogram profile, therefore a single threshold level (static level thresholding) for every image from every experience would not yield a good noise reduction performance.

Matlab's Otsu dynamic threshold proved simple and effective in reducing noise level according to each image's distinct gray level histogram, and it was ultimately used.

Variance filter was also tested in a pre-analysis context (Figure 4.1). This is a filter that allows regions border's detection. However, border detection at this analysis level was not the most helpful method, given that border definition was very fuzzy and didn't allow clear region distinction - it proved more helpful for shape refinement at a higher image analysis level.

Figure 4.2 shows an example of how static level thresholding reduces image noise level. Along the yellow line (going through the third Purkinje reflection), there is significant gray value reduction after threshold. This results, however, were not consistent for every image, many times eliminating third Purkinje reflections when they were fainter.

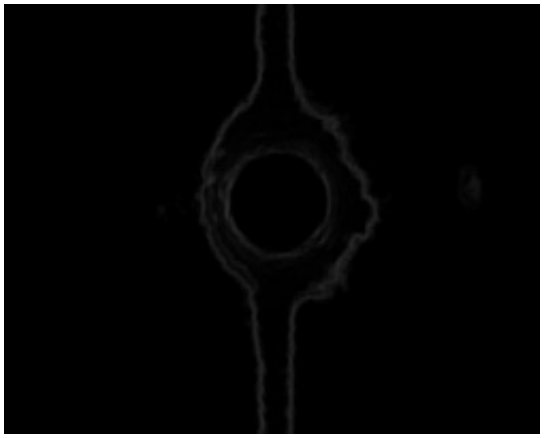

Figure 4.1: Variance filter on original image.

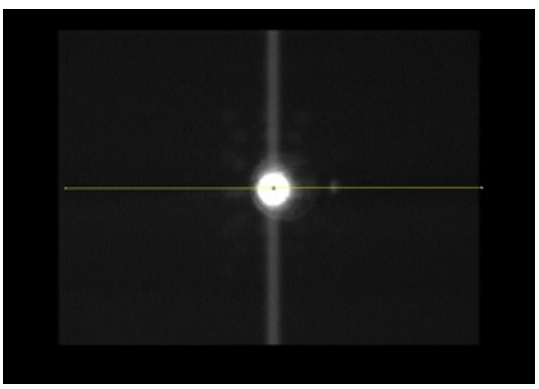

(a) Original image.

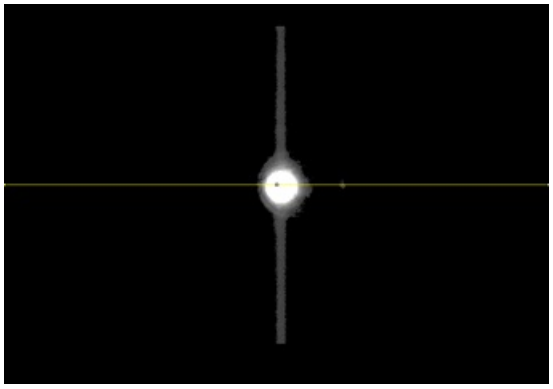

(b) After threshold.

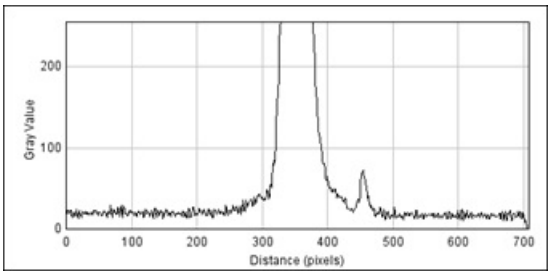

(c) Gray value before threshold.

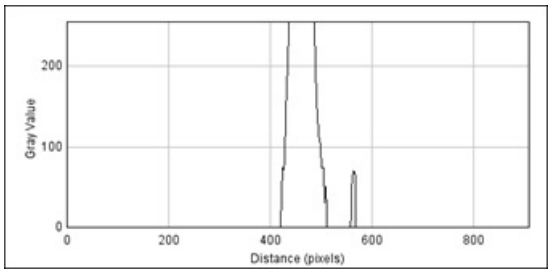

(d) Gray value after threshold.

Figure 4.2: Gray image values along depicted yellow line, before and after static level thresholding.

4.1.2 Detecting the Third Purkinje Reflection

4.1.2.1 Object Detection in Matlab

After thresholding, there is a sharper distinction of meaningful objects.

Matlab provides a pixel aggregation method that groups pixels together based on their closeness. In this way, adjacent non-zero pixels form an object (Figure 4.3). Therefore, an object is a region within an image where all pixels have pixel intensity different than zero. However, inside a given area there can be many different pixel intensity regions.

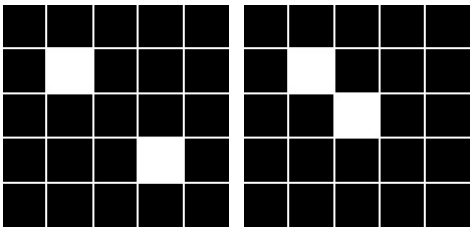

(a) 2 objects detected. (b) 1 object detected.

Figure 4.3: Connected components object detection.

These areas are called connected components objects. They can now be differentiated from one another within a single image (Shape Differentiation approach) or along a series of images (Foreground/Background Differentiation approach). The first approach relies on shape, size or pixel intensity differences of all the different objects in one image, the latter aims at spotting moving objects within a set of images.

Both approaches have been extensively researched in the field of image analysis. The following sections list the ones that were tested for this project's purpose.

4.1.2.2 Foreground/Background Differentiation

Foreground/background differentiation methods are very popular in order to detect moving objects within a set of images [4],[**?**],[6],[19],[20]. Some researched methods were:

- Frame difference [21];
- frame averaging;
- inter-frame connectivity;
- using Normalized Cross-Correlation (NCC) to detect regions with most movement [11],[18].

Table 4.1 summarizes these methods' algorithms and the main reasons why they were ineffective.

Other tested methods were Gaussian Mixture Model based tracking [12] and variance filter along a number of images. These approaches, however, took too much computing time and no results were actually achieved.

Table 4.1 Methods and main results for background/foreground differentiation approach.

Method	Approach	Results	
		Computation Time	Detection Effectiveness
Frame Difference	• For each frame pair, make image difference; • only accept pixels with intensity>threshold intensity, t.	Average	• Aberration objects move or appear/disappear faster than 3rd Purkinje itself; • object/region detected is aberration instead of 3rd Purkinje.
Frame Averaging	• Take n frames before and after current frame (n=2,3); • make current frame average of this frame sequence.	High	
NCC	• For each frame pair, crop within area of interest (reduce computation time); • divide both images into nxm segments; • calculate NCC between corresponding, frame segments • keep segment with lowest NCC (section where most movement occured).	Very high (even with area of interest cropping)	
Inter-frame Connectivity	• Connected-components object detection in each frame; • take previous frame, check inter-frame connectivity between all objects in each frame; • only accept objects that don't have connectivity between frames.	Average	Intra-frame connectivity (i.e., many objects, including 3rd Purkinje, being coupled with background/aberration objects) makes this method obsolete

(a) Previous frame. (b) Current frame.

Figure 4.4: Detected objects for inter-frame connectivity.

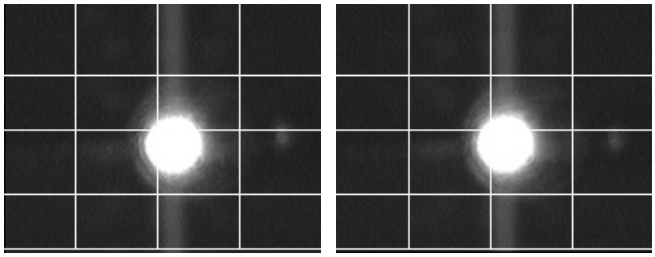

(a) Previous frame. (b) Current frame.

Figure 4.5: Original frames example considered for NCC. Grid pattern for NCC also shown. First Purkinje reflection can be seen to move slightly.

4.1.2.3 Shape Differentiation

Another possibility to differentiate the third Purkinje reflection from other detected objects within an image would be its size, shape or pixel intensity profile.

The third Purkinje reflection pixel intensity profile changes dramatically within a set of images, sometimes being very faint and barely distinguishable from the background, other times having a rather self-differentiating pixel intensity. Whereas the first Purkinje reflection always has the same high intensity pixel value, this feature could not adequately differentiate third Purkinje reflections.

The third Purkinje reflection's size also proved to be an inadequate differentiating feature. This is also a consequence of its changing pixel intensity profile - a smaller third Purkinje reflection usually derives from lower pixel intensities.

Matlab provides an Eccentricity measurement for connected components within an image. It measures whether an object is more closely shaped to a line segment (Eccentricity=1) or a circle (Eccentricity=0). However, as shown on Figure 4.6, third Purkinje reflection's shape changes considerably, therefore not allowing to be detected in this way.

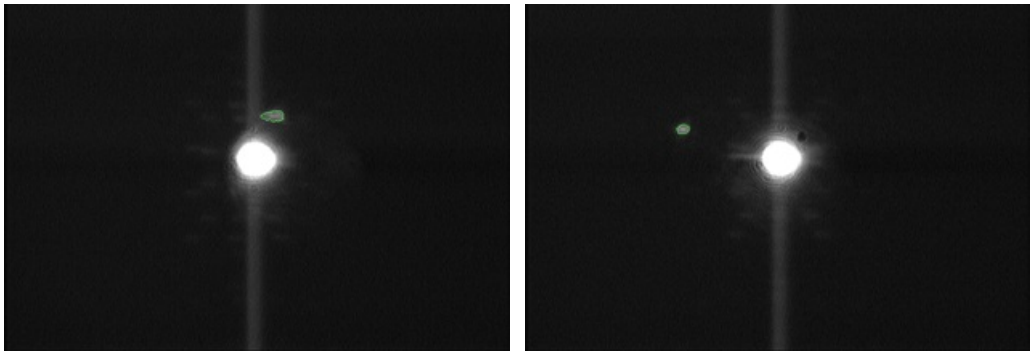

(a) Larger and elliptical-shaped. (b) Smaller and round-shaped.

Figure 4.6: Detected third Purkinje reflections.

Shape differentiation through Eccentricity measurements was also tested for good first Purkinje reflections detection, i.e., to discard images where the first Purkinje reflection was distorted due to misalignment.

Figure 4.7 shows two distinct first Purkinje reflections. On Figure 4.7(a), we see a reflection created due to poor misalignment, on Figure 4.7(b) there is an acceptable reflection. Eccentricity measurements for both these situations are however very similar; there isn't enough difference to use this feature as a differentiating tool. Similar results happened for third Purkinje reflections differentiation.

(a) Eccentricity=0,4927 (b) Eccentricity=0,4114

Figure 4.7: Eccentricity values to distinguish between first Purkinje reflections.

4.2 Results and Discussion

Figure 4.8 shows an example of detected objects/areas by these methods. The pink areas are detected regions throughout a whole set of images. The white area is the current frame after thresholding.

Analysing this image, it is clear that most of detected areas are where artefacts occur. Most importantly, the white vertical column is the most commonly detected region. There is not a sufficiently high third Purkinje reflection detection rate.

Figure 4.8: Detected regions with movement.

Foreground/background differentiation methods detected fast moving objects within a set of images. Whether with frame averaging, NCC or frame difference, artefacts were the fastest moving objects in an image set. This happened because their borders were constantly changing, at a much higher rate than the third Purkinje reflection.

This meant that artefacts had a high detection rate, whereas the third Purkinje reflection, while detectable, wasn't differentiated at a high enough rate to deem these methods effective. To overcome this problem, a movement speed threshold could be implemented. However, the third Purkinje reflection's movement is very erratic and random, meaning that such a method would most probably be ineffective.

Differentiating third Purkinje reflections based on their pixel intensity profile, size or shape was clearly ineffective, given that none of these features are constant for a third Purkinje reflection (although they are for the first Purkinje reflection).

Given that neither moving speed or shape feature are constant for a third Purkinje reflection, none of these methodologies offered high detection rate of this object in the recorded images.

5 . Results

5.1 Image Analysis

5.1.1 Final Procedure

I. Stored image is read.

Taking the original stored image, reading it into Matlab and cutting time and target position stamp rectangle from the top, so as to not interfere in image analysis.

Figure 5.1 is an example of this procedure: on the right is the original image with time and target position stamp; on the left, the image (referred to as *image*)that is going to be analysed on Matlab.

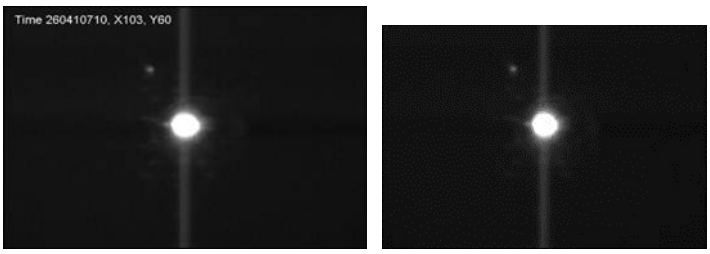

(a) Original image. (b) *image*.

Figure 5.1: Reading image into Matlab.

II. Coarse pixel differentiation - separating first and third Purkinje reflections.

Since the first Purkinje reflection saturates the CCD camera, it can be easily removed in order to increase the contrast of the rest of the image.

Isolating the first Purkinje reflection image indeed proved to be very efficient: simply taking the highest intensity pixels (gray scale value=1, seen in Figure 5.2(a)) on *image* and storing it in an image called *first_purkinje*. This image can, however, still have some random small regions that are also of high intensity. They will be easily removed later, on step **III**.

Detection of third Purkinje reflection will now be done on an image that results from subtracting *first_Purkinje* on *image*. Dynamic thresholding is performed on this difference image, for better differentiation of different pixel intensity regions. The resulting image is called *third_Purkinje* (Figure 5.2(c)).

Figure 5.2 shows normal results for this step.

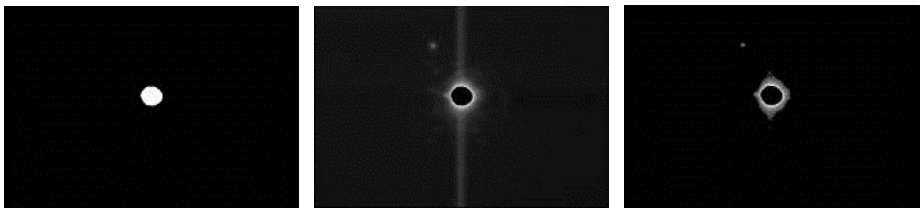

(a) *first_purkinje* (b) *first_purkinje* and *image* difference (c) *third_purkinje*

Figure 5.2: Coarse first and third Purkinje reflections separation.

III. Detecting first Purkinje reflection.

As previously mentioned, *first_Purkinje* may in some cases still have more than one connected component object (which is not the case for this example, Figure 5.3(a), where only one object existed from the beginning). Only the largest object is kept, successfully detecting the first Purkinje reflection.

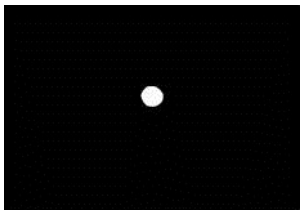

(a) *first_purkinje*.

Figure 5.3: Isolating first Purkinje reflection.

IV. Cropping within area of interest.

Cropping *first_Purkinje* within an area of size 280 x 280 pixel centred on the detect first Purkinje reflection's centroid (Figure 5.3(a)). *third_Purkinje* (Figure 5.4(b)) is cropped around the same area.

This prevents detection of regions that could be mistaken by the algorithm as third Purkinje reflections, but appear much farther away from the first Purkinje reflection than the third Purkinje reflection could.

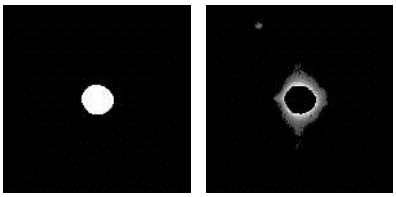

(a) *first_purkinje* (b) *third_purkinje*

Figure 5.4: Cropping area of interest.

V. Third Purkinje reflection detection.

third_Purkinje still has many connected components that need to be discarded.

No shape, size or pixel intensity criteria can be used (as previously discussed in section 4.1.2.3), therefore only objects that are too big to be a third Purkinje reflection are removed. In this way, objects bigger than a normal first Purkinje reflection are ignored.

Through a few steps of image erosion and dilation, objects boundaries are more defined and smaller objects are gradually removed. Objects that are still too small (formed by less than 120 pixel), are now removed, much like when detecting only one first Purkinje reflection.

Figure 5.5(a) is an example where, after removing objects too big and smaller objects, only one object remained.

(a) *third_purkinje*

Figure 5.5: Isolating third Purkinje reflection.

VI. Final third Purkinje reflection detection criteria.

Most of the times, *third_Purkinje* still has more than one object after the previous step. Studying these images, most of the non-third Purkinje objects detected were segments of the vertical white column artefact (Figure 5.6(a)). Therefore, an implemented final criteria for better third Purkinje reflection detection was to remove all objects whose centroid was horizontaly too close to the detected first Purkinje reflection's centroid.

Figure 5.6(a) is an example of a detected object that clearly is not a third Purkinje reflection. In this case, no reflection is detected, even though one is clearly seen below the first Purkinje reflection but hovering over the white vertical column. Since it was not differentiated from the vertical white column in previous steps, it will not be detected.

Figure 5.6(b) is an example of an object that can be kept, because its centroid was not too close to the first Purkinje reflection's centroid.

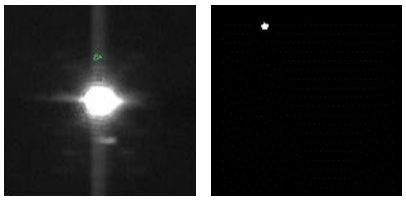

(a) Reject. (b) Accept.

Figure 5.6: Third Purkinje reflection detection final criteria.

5.1.2 Detection Problems

One problem that still occurs is some third Purkinje reflections are detected when there is misalignment of illumination beam and eye's optical axis.

As previously discussed, attempts at discarding situations where misalignment occurs were not possible (section 4.1.2.3), with shape differentiation. No other method proved to be efficient. Therefore, there are still situations where detection can occur in misalignment, as seen in Figure 5.7.

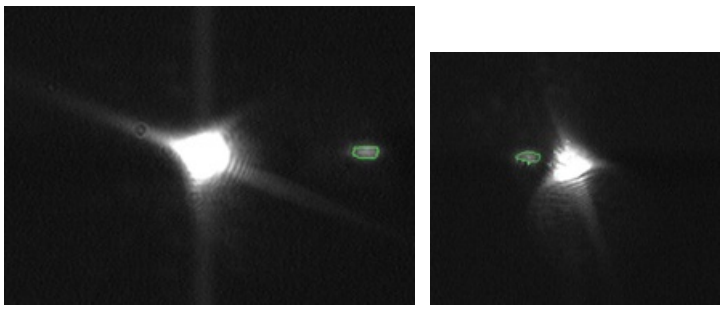

(a) (b)

Figure 5.7: Detection in misalignment.

Finally, other occasional detection problems occur that are not so easily avoidable. An example of this is Figure 5.8. In this case, an object smaller than a first Purkinje reflection whose centroid was not horizontally close to the first Purkinje reflection was detected. However, it was clearly not a third Purkinje reflection.

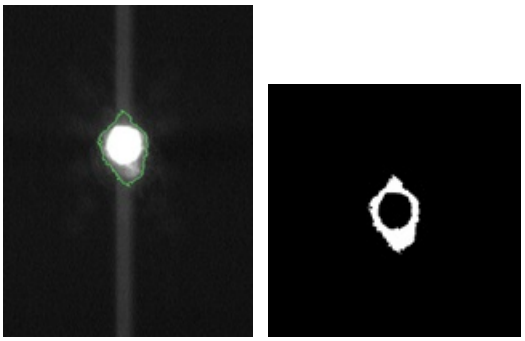

(a) Incorrectly detected third Purkinje. (b) Detail, after subtraction of first Purkinje.

Figure 5.8: Other detection problems.

5.2 Automatic Target Positioning

5.2.1 OLED Rotation

Three subjects were used for calculation of OLED rotation inside the AC Master. The results are in Table 5.1.

Accordingly, $\overline{\phi} = 16{,}7^{\circ}$ was used for calculations that called for this angle.

Table 5.1 Measurements and results for OLED rotation angle calculations.

Subject	First				Last				ϕ
	X1	Y1	X2	Y2	X1	Y1	X2	Y2	
#1	20	30	150	30	49	107	150	30	12,3
#2	20	30	150	30	47	105	150	30	11,5
#3	20	30	150	30	54	96	150	30	26,3

5.2.2 Purkinje Reflections Separation vs. Eye Tilt

5.2.2.1 Angle Step Calculation

A third Purkinje reflection from the test eye can be seen when $\theta \in$ [-1,7; 1,7]°. This is a very small range, and the goniometer's scale did not allow registering every angle's position for each step.

Using Equation 3.2, every angle θ step could be calculated in order to derive a better eye tilt vs. third Purkinje reflection location relationship. Table 5.2 shows these results for both horizontal and vertical tilting.

Table 5.2 Measurements and results for angle step calculations.

	θ_1	θ_2	s_1	s_2	$\Delta\theta$	Δs	θ_{step}
Horizontal Movement	0,2	1,6	1	19	1,4	18	0,08
	1,6	0,2	20	41	-1,4	21	-0,07
	-0,4	-1,7	42	58	-1,3	16	-0,08
	-1,7	-0,2	59	74	1,5	15	0,10
Vertical Movement	-1,7	-0,5	1	17	1,2	16	0,07
	0,2	1,7	18	32	1,5	14	0,11
	1,7	0,4	33	56	-1,3	23	-0,06
	-0,5	-1,7	57	79	-1,2	22	-0,05

5.2.2.2 Analysing the Results

Performing image analysis on the recorded images allowed calculating the distance between first and third Purkinje reflections with every change in angle.

Figure 5.9 shows how tilting the test eye changed the third Purkinje reflection location. Both horizontal and vertical tilting were tested. From this figure, we also calculate that the third Purkinje visibility radius around the first Purkinje reflection is 83 pixels.

Furthermore, in order to have a better estimation on the eye tilt and Purkinje reflections separation relationship, individual back and forth sets of points were separated for Figure 5.10. Reflections separation are plot for increasing eye tilt (absolute tilt angle). In this way, it was possible to perform linear regression on every similar set of points, obtaining linear coefficients k and b shown on Table 5.3. Variables d and θ are therefore taken as linearly related according to,

$$d = k \cdot \theta + b \tag{5.1}$$

Figure 5.10 also plots function f(θ)= $\bar{k} \cdot \theta + \bar{b}$, in order to evaluate the linearity of Purkinje reflections separation for every angle tilting.

The following chapter (specifically, section 6.2.1) will discuss these plots' linearity. For reasons that will be then further explained, it is useful to take θ in radians instead of degrees. Plotting the Purkinje reflections separation for θ in degrees or radians causes no change to its behaviour, since a linear relation exists between these units. Table 5.3 shows that indeed only the linear plot's inclination changes, when using θ in radians or degrees. Therefore, all of the following analysis plots will present θ in radians.

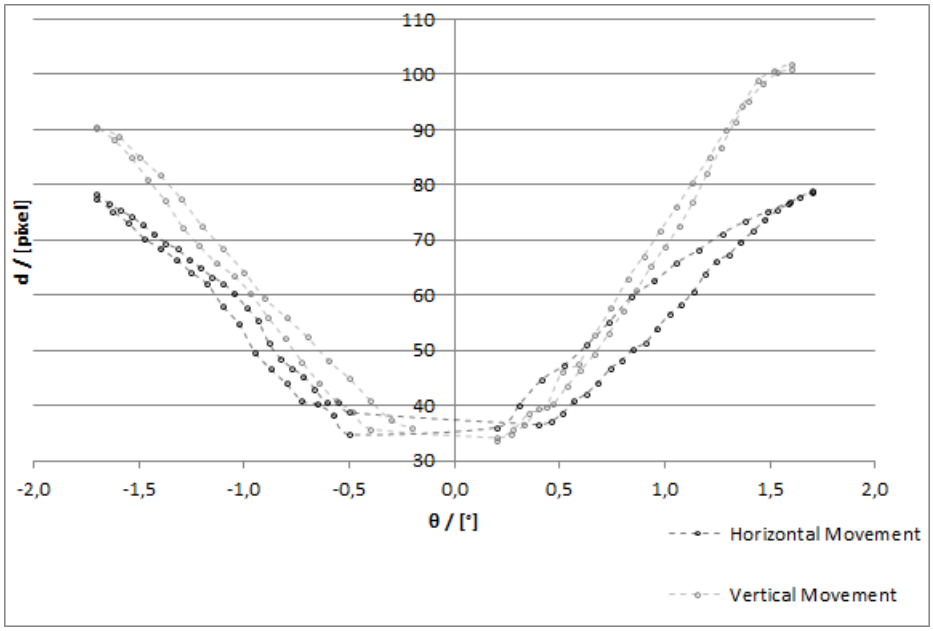

Figure 5.9: Separation between first and third Purkinje reflections as a resul of test eye tilting.

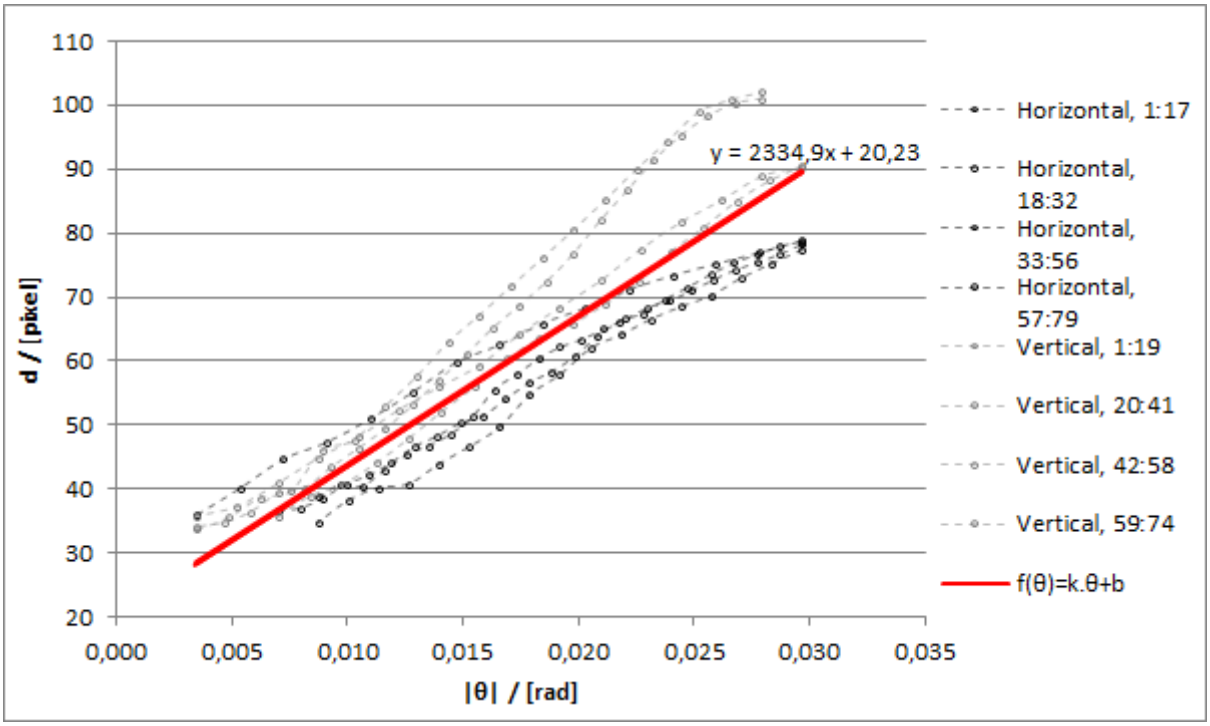

Figure 5.10: Distance vs. Absolute angle.

Table 5.3 Linear regression coefficients for horizontal and vertical movements' plots.

	Points	Linear Coefficients		
		k / [pixel /°]	k / [pixel/rad]	b / [pixel]
Horizontal Movement	1:17	37,18	2130,2	15,84
	18:32	28,98	1660,5	32,91
	33:56	35,24	2019,3	20,78
	57:79	34,79	1993,2	21,39
Vertical Movement	1:19	53,79	3081,7	19,05
	20:41	53,59	3070,3	16,96
	42:58	43,43	2488,0	17,26
	59:74	39,03	2236,2	25,66
Statistics		$\bar{k}$=40,8 σ (k)=8,4	$\bar{k}$=2335 σ (k)=480	$\bar{b}$=21,2 σ (b)=5,3

5.2.3 Eye Fixation Deviations

Three videos were recorded and subject to image analysis. Although the eye was gazing at a fixed target, the third Purkinje reflection is clearly moving. Figure 5.2.3 shows two image frames from a video, where it can be clearly seen that the detected third Purkinje reflection moved. Figure 5.11 shows the overall movement of the reflection during a section of one of these videos, reflecting the same behaviour.

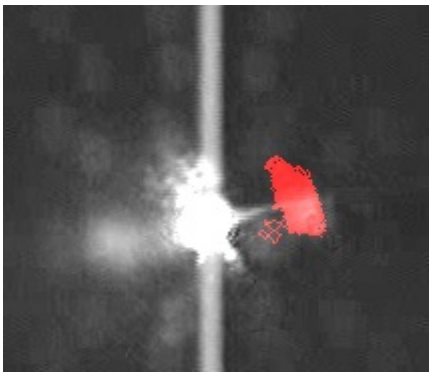

Figure 5.11: Detected third Purkinje reflection's location with fixed target.

Table 5.4 Statistics for third Purkinje location as the eye looks at a fixed target.

Video	Average		Standard Deviation	
	$\bar{X}$	$\bar{Y}$	$\sigma(X)$	$\sigma(Y)$
1	360,6	182,5	5,94	10,97
2	249,2	168,8	15,26	21,09
3	282,0	155,2	40,93	20,55
Overall	318,9	176,6	54,4	17,5

5.2.4 Final Calculations

Assuming a linear relationship as the eye tilts and the Purkinje reflections separation, and using Equation 3.13, the following figures show the calculated adequate target locations, along with the original target locations from which the new ones were calculated.

Figure 5.12 zooms in for more detail where most of the spots are within the 650x480 pixel OLED. Also represented are error bars which arise from uncertainty of eye fixation for a target location. The error bars X and Y amplitudes come from statistics of eye fixation deviations, introduced in Section 5.2.3 ($\sigma(X)$ and $\sigma(Y)$ values from Table 5.4). They will allow further analysis, on whether the calculated target's are within an acceptable error range.

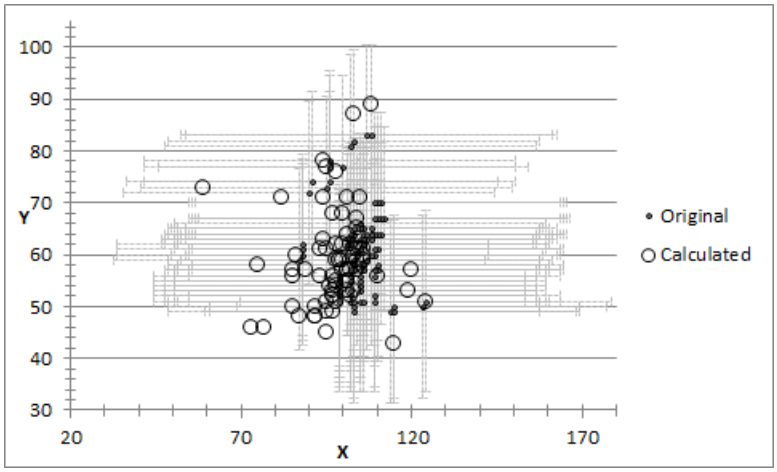

Figure 5.12: Calculated vs. Original target locations, detail.

6. Discussion

6.1 Image Analysis

Performing image analysis on this project dealt mainly with avoiding detecting incorrect third Purkinje reflections. The great majority of detection errors and difficulties were due to the vertical white column artefact (Figure 3.6(b)). Having a CCD camera that does not give rise to the blooming effect would greatly improve detection efficiency. Furthermore, other simple image analysis methods (such as frame differencing - as mentioned in Chapter 4) could achieve better results with a more straightforward approach.

For this procedure, an important feature to analyse is how often a third Purkinje reflection is detected. Table 6.1 shows, for every experience, the original number of images, the number of images with detected third Purkinje reflections, and also how many target points could be calculated.

Table 6.1 Third Purkinje detection and adequate target location calculation efficiency rates.

Frame Set	#Frames		Calculated Points	Efficiency Rate (%)	
	Originally	3rd Purkinje Detected		3rd Purkinje Detection	Point Calculations
#1	176	29	15	16,5	8,5
#2	82	11	4	13,4	4,9
#3	80	16	10	20	12,5
#4	97	11	2	11,3	2,1
#5	260	10	4	3,8	1,5
#6	260	22	9	8,5	3,5
#7	260	21	11	8,1	4,2
#8	238	31	19	13,0	2,0

Third Purkinje reflection's detection efficiency is therefore very low. Despite the fact that the user can see its presence in almost half of the frames on average, detection for a given experiment falls on the 10% range. This is a very hindering feature; detection efficiency should be very high for normal patient conditions such as these experiments, because real case conditions where patients will suffer from other problems that lower detection.

Another important feature to take note is that images taken with first Purkinje reflection misalignment are not distinguishable with this method. In fact, after analysing all images in an experiment, the final results would have to be reviewed again in order to individually rule out frames in such conditions.

In summary, it can be said that:

- A single artefact present in every image changes the whole project's approach to image analysis;
- in consequence, image analysis is very inefficient due to this object's pixel intensity profile similarity with the desired objects;
- detection of incorrect third Purkinje reflections still occurs, requiring post-image analysis review of the results from an operator that has experience with this phenomenon.

6.2 Automatic Target Positioning

Analysis of Figure 5.12 clearly shows that this approach does not result in consistent adequate target locations for alignment. In this section, some reasons that can explain this behaviour will be discussed.

6.2.1 Purkinje Reflections Separation vs. Eye Tilt

One thing to analyse is the relationship between eye tilt and third Purkinje reflection location. In this project, we assumed a linear relationship based on the experience with the test eye (section 5.2.2). Analysing Figure 5.10, we see that, although a linear plot given by Equation 5.1 does seem to follow the general behaviour of the Purkinje separation, some fluctuations can be seen.

Given that the test eye's third Purkinje reflection was very similar in intensity with the first Purkinje reflection (Figure 3.16(a)), therefore much more distinguishable than its human eye counterpart, this stage's image analysis' detection errors are not accountable for these deviations.

Most probably, these behaviour differences occur because the relation is simply not strictly linear. [7] suggests a sinusoidal relationship of the type,

$$d = 7\sin(\theta)(mm) \tag{6.1}$$

However, for these experiments, the angle data were very small ($\theta \in$ [-1,7;1,7]$^\circ$). Given the trigonometric identity,

$$\lim_{\theta \to 0} \frac{\sin(\theta)}{\theta} = 1 \tag{6.2}$$

for θ in radians. We have that, for our θ (in radians) data range,

$$\theta \simeq \sin(\theta) \tag{6.3}$$

therefore no difference between a linear behaviour and one defined by Equation 6.1 is expected.

Figure 6.1 shows that indeed θ and sin (θ) are the same for such small angles. Also, g(θ) is intentionally not-superimposed on f(θ) for better viewing. Therefore, it is shown that a linear relationship is the most simple description of these experiments. These deviations, however, appear to occur rather randomly, which signifies that they are due to involuntary eye movements.

Furthermore, there aren't constant linear coefficients between and within experiments, making this approach an obstacle to take into account in achieving this project's goal.

Also, we have to consider that these measurements were taken for strictly horizontal and vertical eye tilting, which could almost never be expected to happen with a human eye experiment. Therefore, there is still a question of whether the reflections' separation would behave even more erratically for tilting movements that are combinations of vertical and horizontal movements.

More experiments will have to be performed in order to achieve better modelling, perhaps finding an average population model.

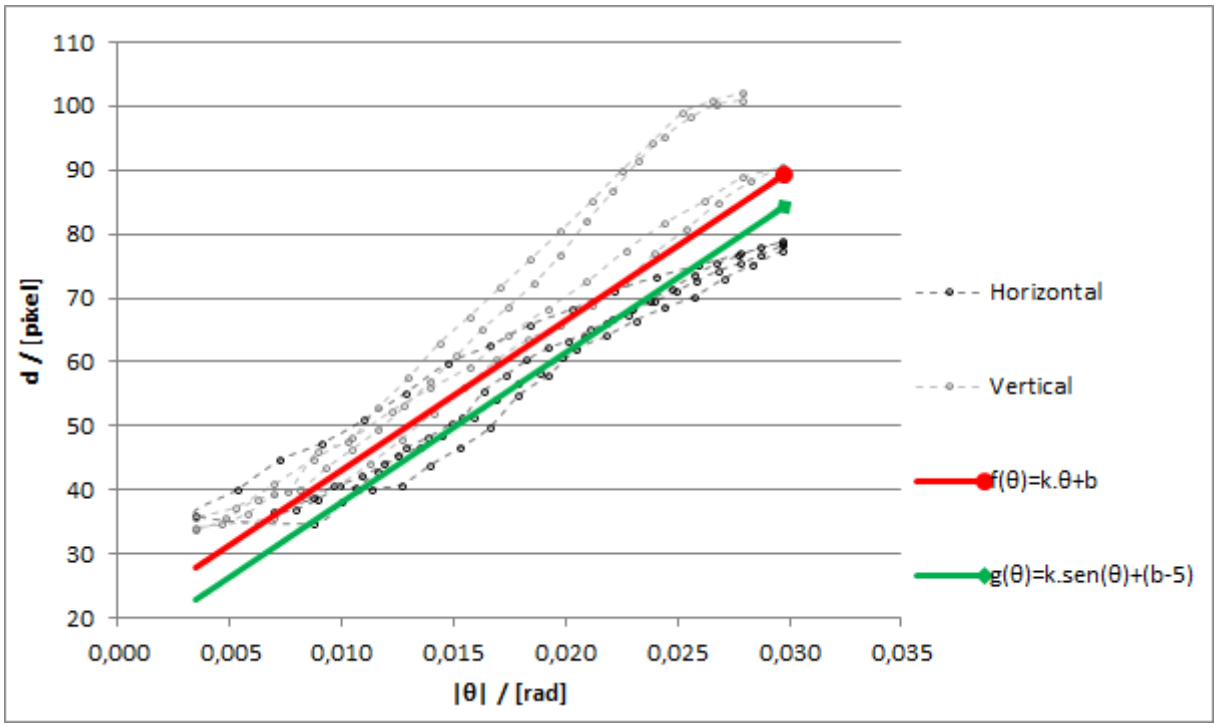

Figure 6.1: Comparing separation vs. absolute angle tilt with θ and sin (θ) plots.

6.2.2 Final Calculations

Analysing Figures **??** and 5.12, it is clear that the derived equations for adequate target position calculations (Equation 3.13) do not provide a single adequate target location (as is in fact expected due to the natural eye motion even during fixation), rather a set of locations. This project's ideal goal was based on the idea that the calculated adequate fixation position would be unique for each patient (or at least up to the error boundaries of the eye's motion).

An important result is the comparison of the obtained fixation locations and the corresponding Purkinje reflections with the statistical error boundaries. It is however seen, that the dispersion of the obtained Purkinje images is slightly bigger than expected from studies based on a single fixation target position. These results help, however, in narrowing down the region where the target should be moving, in order to detect third Purkinje reflections more efficiently. They would have to be tested to see if they provide alignment where third Purkinje location is closer to the first.

There are some improvements that can be done for this movement modelling.

First, as discussed on the previous section, the actual Purkinje reflection's separation behaviour as the eye tilts is very difficult to model. Results show that there is great deviation that does not seem to be accountable into a simple function form. Therefore, since the derived final calculations rely on a linear behaviour, they do not perform well given that this behaviour may be linearly based, but is however not constant. Further experiments and studies are needed to correctly model the reflections' separation behaviour as the eye tilts. Its corresponding function can be easily be integrated into Equation 3.4.

Another situation that can lead to calculation errors is timing accuracy between the patients' fixation on the new target location and the image recording.

Initially in this project, Purkinje reflections video was recorded instead of still images for every target position change (section 3.3.2). Since consistent detection of third Purkinje reflections overlapping the first Purkinje reflection was not possible in a video, another procedure would have to be implemented.

The current procedure works in a way to mitigate this problem: an image is recorded whenever the target changes position. This, however, gives rise to the problem that when the image is taken, perhaps the eye is not actually looking at the intended spot, and probably still moving toward focusing on it. In practice, the associated eye fixation error would be increased even more.

To solve this problem, instead of recording a single image when the target changes location, a series of images could be recorded while the target is standing still. This way, the average third Purkinje location for each target hiatus is calculated and whenever the deviation is too large, that time frame would be ignored in the calculations.

Since all the detected third Purkinje reflections were manually reviewed in order to eliminate incorrect detections that would not be useful for final calculations, the detection method is not accountable for dispersion in these results.

Summarizing, the calculated target locations gave rise to larger dispersion of the third Purkinje reflection, as was expected from error estimations based on experiments of a single target location. The reason for this deviation might be:

- inaccurate Purkinje reflections separation vs. eye tilting behaviour modelling - further experimentations are required to improve the model;
- timing accuracy between detected third Purkinje reflection and actual fixation target location - accepting target hiatus's time frames with low third Purkinje location dispersion improves this aspect.

7 . Conclusions and Future Work

This project's goal was to research whether an image analysis approach to automatically detect third Purkinje reflections could help provide adequate fixation target location for interferometry measurements of anterior eye chamber.

Several image analysis approaches were tested to detect and follow the third Purkinje reflection's location as the eye moved, eventually detecting when it overlapped the first Purkinje reflection. However, an artefact present in every image prevented correct reflection detection on a whole experiment, given that its intensity profile was very similar to the reflection's and its boundaries movement's weren't neglectable. A new camera model is therefore planned, that is free from those blooming artifacts. In this case, the developed algorithms will provide proper delineation of the Purkinje reflections.

Another approach was devised, that relied on knowing how the third Purkinje reflection moved as the eye tilted. Therefore, the inability to follow the third Purkinje reflection along the whole experiment could be surpassed. Taking its movement model, any given pair of detected third Purkinje reflections would allow extrapolation of where the target should be placed so that the reflection would overlap the first Purkinje reflection. Assuming regularity in this behaviour for a given person, the calculated target location should be unique, up to the natural fixation inaccuracy given by the patients eye motion. Those fluctuation boundaries have been determined based on a statistical model for a single fixation location.

The calculated fixation spot location was precise enough to detect the third Purkinje image. This statistical spread due to the natural eye motion obtained by repeated reconstruction of the location was slightly larger than expected from the statistical analysis of a single fixation spot. Further experiments would have to be undertaken in order to determine if these results provide smaller reflections' separation than the original points. They also enable, however, narrowing of the target's scanning pattern to a region with higher third Purkinje reflection's detection rate. This feature is especially important for subjects whose pre-alignment setup (section 3.2) encounters difficulties in finding a third Purkinje reflection.

The larger dispersion of the Purkinje image location might also be due to a non-linear relation between the fixation spot location and the Purkinje reflection for larger angles, depending also on the relative head position, as well as on time delay between the image recording and the actual fixation. A series of improvements can be implemented in order to diminish these factors effect on dispersion.

As already stated above, a device whose CCD camera doesn't saturate on a central vertical stripe is already available, and further research will have to perform image analysis on images without this artefact. Simple frame differentiation or background subtraction could be then implemented, eventually even allowing discarding of misaligned first Purkinje reflection images.

Regarding the procedure, as mentioned previously, further experiments in modelling third Purkinje's reflection movement with eye tilting are still required. Since involuntary eye movements lead to a high degree of fluctuations, an average population model can be considered.

Detecting target hiatus' time frames with low third Purkinje dispersion will also improve calculated target's dispersion.

A strong conclusion in this project is that Purkinje reflections overlap occurs very rarely. The procedure will have to more strongly rely on the model for the third Purkinje's reflection movement.

As an important conclusion, the major challenge of optimizing the measurement procedure is the natural fluctuation of the Purkinje reflections, whose error boundaries are already close to the limits of actually enabling reasonable interferometric measurements.

There is a need for a more robust alignment procedure yielding better results exists. Automation would allow specialized operators to be removed from the equation and reduction of implementation costs, thus enabling this equipment and more accurate interferometry measurements to reach as many people as possible.

Bibliography

[1] M Akhlaghi and A Najafianjazi. Comparison of ultrasound and optic biometry with respect to eye refractive errors after phacoemulsification. *Journal of Research in Medical Sciences*, 13(2):43–47, 2008.

[2] AMO. Outcome Optimization with Accurate Biometry. Technical report, Advanced Medical Optics, Inc., Santa Ana, 2007.

[3] A Castro, P Rosales, and S Marcos. Tilt and decentration of intraocular lenses in vivo from Purkinje and Scheimpflug imaging Validation study. *Journal of Cataract Refractive Surgery*, 33:418–429, 2007.

[4] M K Cheezum, W F Walker, and W H Guilford. Quantitative Comparison of Algorithms for Tracking Single Fluorescent Particles. *Biophysical Journal*, 81(4):2378–2388, 2001.

[5] A Chennu. Optical Coherence Tomography - A Literature Survey. Technical report, Heriot Watt, 2008.

[6] S S Cheung and C Kamath. Robust techniques for background subtraction in urban traffic video. *East*.

[7] M R Clark. A two-dimensional Purkinje eye tracker. *Behavior Research Methods*, 7(2):215–219, 1975.

[8] S Dawson, S Hogan, R Kirk, and M Paterson. Optical biometry using partial coherence interferometry prior to cataract surgery. Technical Report March, Medical Services Advisory Committee, Department of Health and Ageing, Canberra, 2003.

[9] W Drexler, A Baumgartner, O Findl, C K Hitzenberger, H Sattmann, and A F Fercher. Submicrometer Precision Biometry of the Anterior Segment of the Human Eye. *Investigative Ophthalmology*, 38(7):1304–1313, 1997.

[10] W Drexler, O Findl, R Menapace, G Rainer, C Vass, C K Hitzenberger, and A F Fercher. Partial Coherence Interferometry: A Novel Approach to Biometry in Cataract Surgery. *American Journal of Ophthalmology*, 9394, 1998.

[11] J Gao. The Maximum Cross-Correlation approach to detecting translational motions from sequential remote-sensing images. *Computers & Geosciences*, 22(5):525–534, June 1996.

[12] P Kaewtrakulpong and R Bowden. An Improved Adaptive Background Mixture Model for Real- time Tracking with Shadow Detection 2 Background Modelling. *Online*, pages 1–5, 2001.

[13] C Kent. The Anterior Chamber, From Every Angle. *Review of Ophthalmology*, pages 1–2, 2005.

[14] A K Khurana. *Theory and Practice of Optics and Refraction*. Elsevier, 2nd edition, 2008.

[15] T Kohnen, editor. *Modern Cataract Surgery*. Basel, 2002.

[16] B Lackner, G Schmidinger, and C Skorpik. Validity and Repeatability of Anterior Chamber Depth Measurements With Pentacam and. *Optometry and Vision Science*, 82(9):858–861, 2005.

[17] H M Merklinger. Addendum to Focusing the View Camera, 1995.

[18] M S Nagmode, M A Joshi, and A M Sapkal. A Novel approach to Detect and Track Moving Object using Partitioning and Normalized Cross Correlation. 9(4):49–56, 2009.

[19] N S Naraghi. A Comparative Study of Background Estimation Algorithms. (September), 2009.

[20] R J Radke, S Andra, O Al-kofahi, and B Roysam. Image Change Detection Algorithms : A Systematic Survey. *Sensing And Imaging*, pages 1–32, 2004.

[21] M H Sigari, N Mozayani, and H R Pourreza. Fuzzy Running Average and Fuzzy Background Subtraction : Concepts and Application. *Journal of Computer Science*, 8(2):138–143, 2008.

[22] Zeiss Meditec AG. AC Master Software Version 1.xx, 2004.